Review | Open Access

Microstructures

Kim *et al. Microstructures* **2026**, *6*, 2026062 **DOI:**10.20517/microstructures.2025.148

Gradient engineering in functional complex oxide heterostructures

Sanghyeon Kim#, Younji Kim#, Daesu Lee

Keywords:
Strain gradient, chemical gradient, electric field gradient, flexoelectricity, complex oxide

Citation: Kim, S.; Kim, Y.; Lee, D. Gradient engineering in functional complex oxide heterostructures. *Microstructures* **2026**, *6*, 2026062. https://dx.doi.org/10.20517/microstructures.2025.148

Received: 31 Oct 2025 **First Decision:** 19 Dec 2025 **Revised:** 16 Jan 2026 **Accepted:** 13 Feb 2026 **Published:** 15 May 2026

Academic Editor: Houbing Huang
Copy Editor: Ping Zhang
Production Editor: Ping Zhang

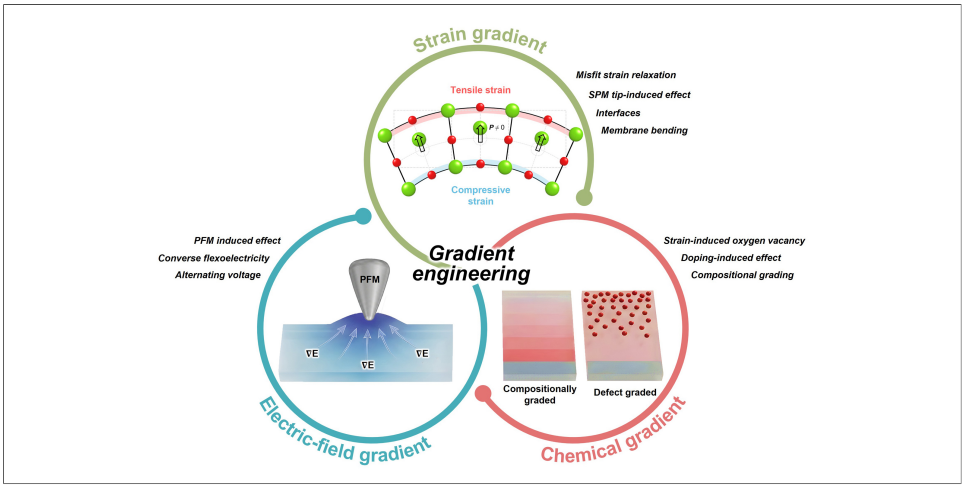

Abstract

Gradient engineering represents a revolutionary framework for the design of functional complex oxide heterostructures with properties beyond those achievable in homogeneous bulk materials. Emerging from research on strain gradients and flexoelectricity, this paradigm has been extended to include field and chemical gradient strategies. Pioneering research has demonstrated that flexoelectricity can induce ferroelectric-like behavior in centrosymmetric materials and impart various functionalities, including the flexo-photovoltaic effect and functional domain walls. This breakthrough has established strain gradients as powerful design parameters and has inspired the exploration of other gradient types in oxide systems. This article provides a comprehensive review of various types of gradient engineering, including strain, field, and chemical gradient engineering, focusing on their origin, methods of induction, and functionalities. As the field matures, gradient engineering has the potential to advance the development of oxide-based technologies for electronics, energy conversion, and information processing.

INTRODUCTION

Check for updates

The flexoelectric effect, which is defined as the coupling between a strain gradient and electric polarization[1-3], is a universal electromechanical phenomenon

Department of Physics, Pohang University of Science and Technology, Pohang 37673, Korea.
#These authors contributed equally to the work.

Correspondence to: Prof. Daesu Lee, Department of Physics, Pohang University of Science and Technology, Pohang 37673, Korea. E-mail: dlee1@postech.ac.kr

fundamentally distinct from conventional piezoelectricity[4]. While piezoelectric responses require materials that lack inversion symmetry, flexoelectricity can exist in a diverse range of materials encompassing not only dielectrics[5,6], semiconductors[7-9], two-dimensional (2D) materials[10-13], bio-materials[14,15], and even metals[16,17]. This offers the opportunity to induce and control polarization states in a broad range of systems. In particular, complex oxide heterostructures have become the focus of intense research due to their structural versatility, variety of defects, and strongly interacting electronic, magnetic, and lattice degrees of freedom[18,19]. Oxides can also support large strain gradients at interfaces[20], domain boundaries[21], and in the bulk[6], accommodate multiple cation valence states[22,23], and offer tunable oxygen vacancy concentrations[24], thus they represent an ideal platform for the use of flexoelectricity in advanced functionalities.

Recent research has demonstrated that flexoelectric phenomena in oxides can be deliberately engineered to obtain new material properties. For example, strain gradients in epitaxial thin films and nanostructures generate localized polarization fields, enhance charge carrier dynamics[20], and direct ferroic domain formation[25]. Electric field gradients applied through scanning probes or asymmetric device geometries can also modulate flexoelectric responses at the nanoscale[26,27], while chemical gradients arising from compositional tuning or oxygen vacancy distributions can be employed to couple lattice strain with defect chemistry, generating dynamic polarization states[28]. These approaches have produced promising functionalities, including flexo-photovoltaic effects that enhance charge separation and the photoresponse[29,30], catalytic activity modulation through polarization-induced surface chemistry[31], polarization switching and domain tailoring, which enable control over ferroic orders[25,32], emerging fields of flexoelectronics where electromechanical coupling is harnessed for device concepts[9,33], and the control of magnetism and spin textures via flexoelectric fields[17,34,35]. These studies demonstrate the versatility of flexoelectricity as a design principle for the development of next-generation functional oxide materials.

This review aims to provide a systematic summary of flexoelectricity in oxide materials, with particular emphasis on the interaction between structural gradients and functional responses. As shown in Figure 1, we categorize recent advances into three major approaches - strain, electric-field, and chemical gradient engineering - and examine how each method has been employed to produce novel device concepts. Finally, we discuss current challenges and opportunities in the field, highlighting the potential of flexoelectricity as a versatile design for future oxide-based functional materials.

FLEXOELECTRIC EFFECT

Historical background

The term flexoelectricity originates from the combination of “flexus”, meaning bending, and “electricity”, referring to the electric polarization generated under mechanical stimuli. The concept was first proposed by Soviet scientists Mashkevich and Tolpygo in the 1950s, who theoretically predicted that strain gradients in crystals could induce polarization even in centrosymmetric systems[36]. Later in 1964, Kogan phenomenologically formulated flexoelectricity within the framework of continuum electromechanics[37]. These pioneering works laid the theoretical foundation for what is now recognized as a universal electromechanical coupling mechanism.

Following these initial proposals, theoretical models were developed to describe flexoelectricity at the continuum scale and from first-principles calculations[38-40]. In parallel, experimental studies, which were initially limited by measurement sensitivity, confirmed the existence of flexoelectric polarization in various materials, ranging from simple dielectrics to complex oxides[5,41,42]. Advances in thin-film growth, scanning probe microscopy (SPM), and *in-situ* characterization techniques have since accelerated research, allowing

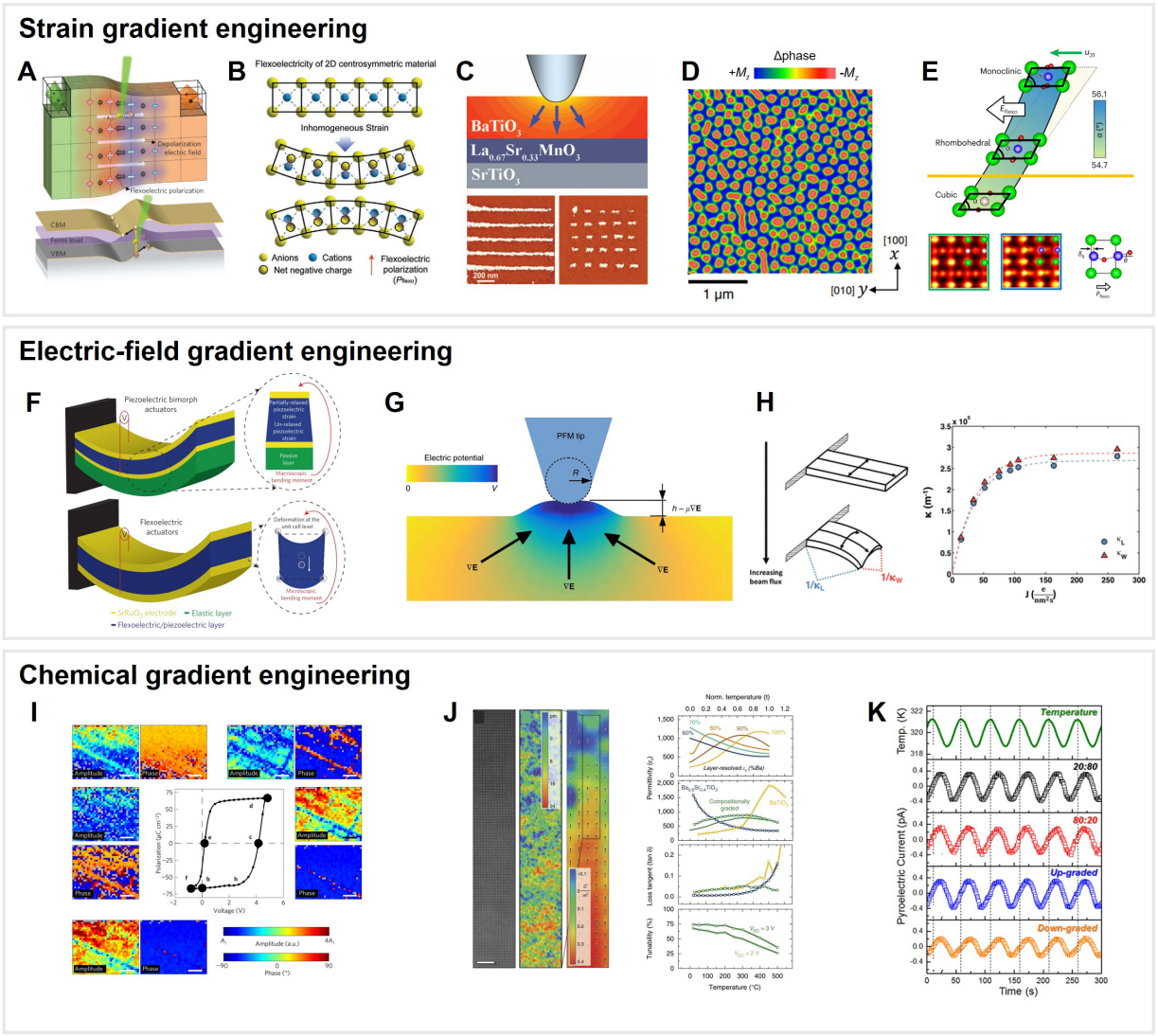

Figure 1. Overview of the classification and functionalities of complex oxide heterostructures based on different gradient engineering strategies. (A-E) Strain gradient engineering. (A) Flexo-photovoltaic effect. Reproduced with permission[20]. Copyright 2015, Springer Nature; (B) Flexocatalysis. Reproduced with permission[62]. Copyright 2023, John Wiley and Sons; (C) Polarization switching and domain tailoring. Reproduced with permission[25]. Copyright 2012, American Association for the Advancement of Science; (D) Magnetic skyrmions. Reproduced with permission[34]. Copyright 2021, American Physical Society; (E) Ferromagnetic polar metal. Reproduced with permission[17]. Copyright 2024, Springer Nature; (F-H) Electric-field gradient engineering. (F) Flexoelectric actuators. Reproduced with permission[27]. Copyright 2016, Springer Nature; (G) Converse flexoelectric effect through piezoresponse force microscopy. Reproduced with permission[26]. Copyright 2019, Springer Nature; (H) Converse flexoelectric effect-induced bending. Reproduced with permission[83]. Copyright 2018, American Chemical Society; (I-K) Chemical gradient engineering. (I) Domain structure engineering. Reproduced with permission[109]. Copyright 2016, Springer Nature; (J) Polarization gradient. Reproduced with permission[108]. Copyright 2017, Springer Nature; (K) Improved pyroelectric effect. Reproduced with permission[106]. Copyright 2013, American Chemical Society. 2D: Two-dimensional.

the direct observation and quantitative evaluation of flexoelectric coefficients at the nanoscale[43].

Theoretical framework and mathematical description

Flexoelectricity can be described phenomenologically by the linear coupling between polarization and a strain gradient as follows[1,44]:

$$P_i = \mu_{ijkl} \frac{\partial u_{jk}}{\partial x_l} \tag{1}$$

where P_i is the induced polarization, μ_{jk} is the strain tensor, and μ_{ijkl} is the fourth-rank flexoelectric tensor. Unlike piezoelectricity, this polarization is not driven by the strain itself but rather by its gradient. As a result, flexoelectric responses are intrinsically linked to local structural inhomogeneity induced by spatial gradients.

First-principles density functional theory calculations have also been widely employed to investigate flexoelectric coefficients and strain gradient-induced polarization at the atomic scale[1,45]. These approaches quantify the magnitude and microscopic origin of flexoelectric responses, complementing continuum-level models and establishing a direct connection between lattice-scale distortion and macroscopic polarization.

At the atomic scale, flexoelectricity arises from two primary contributions: electronic contributions, which originate from the strain gradient-induced redistribution of the electron density, and ionic contributions, which arise from asymmetric atomic displacement that shifts the centers of positive and negative charge. Both contributions can coexist and are strongly influenced by bonding characteristics, lattice stiffness, and dielectric screening, reflecting the material-dependent nature of flexoelectric coupling[1,24].

Within this framework, polarization is a response to spatially non-uniform structural or electrostatic perturbations. While the direct flexoelectric effect corresponds to polarization induced by strain gradients, this form of coupling also gives rise to the converse flexoelectric effect, in which inhomogeneous electric fields or polarization distributions generate mechanical deformation.

This viewpoint provides a unifying basis for the gradient engineering strategies explored in this review. Although strain, electric-field, and chemical gradients arise from distinct physical origins, they all introduce spatial inhomogeneities that can disrupt inversion symmetry and activate flexoelectric coupling. In this sense, different gradient engineering approaches have a common physical basis for the generation of flexoelectric responses and electromechanical functionality in complex oxide materials. Figure 2 schematically illustrates how, despite their differing physical origin, strain, electric-field, and chemical gradients operate on the same flexoelectric coupling mechanism, thus providing the conceptual foundation for the gradient engineering strategies discussed in the following sections.

Characteristics of flexoelectricity

Unlike piezoelectricity, which is restricted to non-centrosymmetric crystals, the flexoelectric effect can, in principle, occur in all materials, independent of the crystal symmetry[1,15]. This universality has been widely demonstrated not only in oxide systems, where centrosymmetric compounds such as $SrTiO_3$ display flexoelectric polarization under strain gradients[5], but also in various other material families, including semiconductors[7-9], 2D materials[10-13], polymers[46,47], and biological materials[14,15]. More recently, flexoelectric responses have even been reported in metals[16,17] and ice[48-50], illustrating that flexoelectricity is not confined to traditional dielectrics but represents a general form of electromechanical coupling that is present in a wide range of matter.

Another important characteristic of flexoelectricity is that the flexoelectric coefficient in ceramics and oxides is often significantly larger than in polymers or semiconductors[51]. The high dielectric permittivity of oxide ceramics strengthens the electromechanical response, making them particularly promising for functional applications. In addition, unlike ferroelectricity or piezoelectricity, which may disappear above a critical temperature, flexoelectricity persists even at elevated temperatures as long as the strain gradient is present[52]. This expands the operational window for high-temperature devices and catalytic processes.

Finally, flexoelectricity is considerably size-dependent. In nanoscale systems, where strain gradients can become extremely large due to curvature, bending, or lattice relaxation, the induced polarization can be orders of magnitude stronger than in bulk systems[1,53]. This scaling behavior means that nanostructured

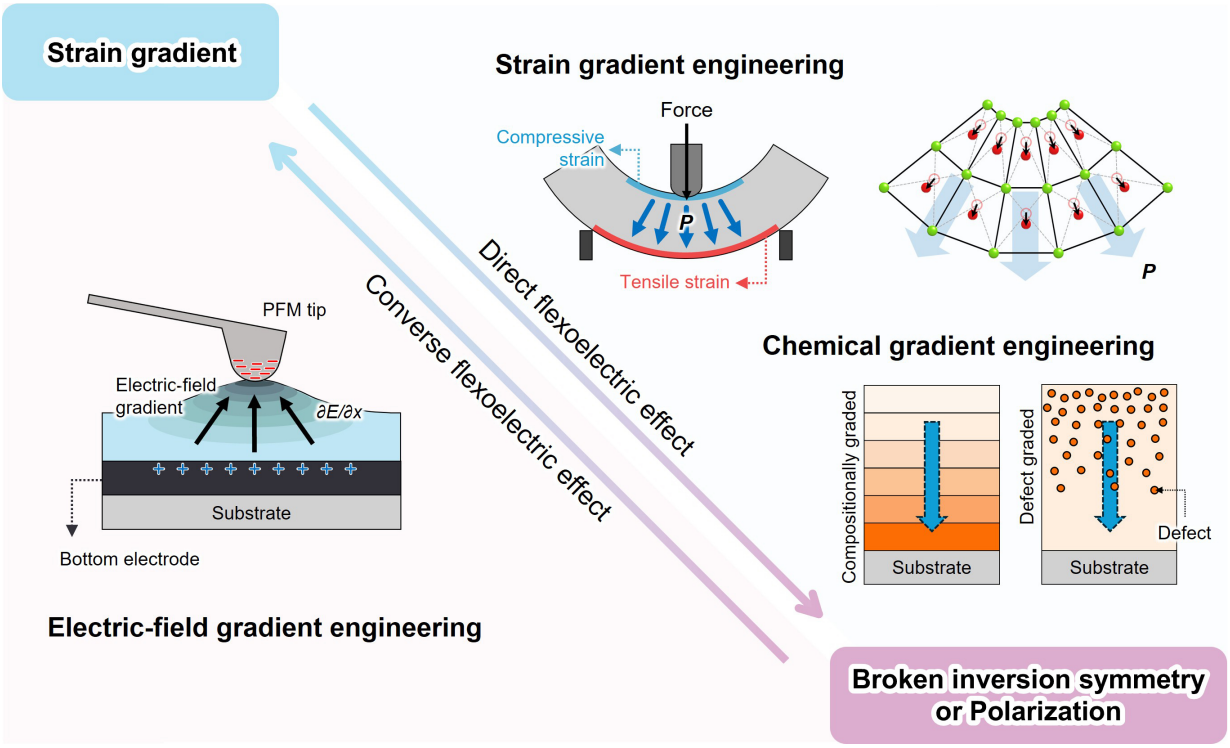

Figure 2. Schematic illustration of the unified physical origin of gradient engineering in complex oxides. Representative strain, electric-field, and chemical gradients are illustrated. PFM: Piezoresponse force microscopy.

oxides such as nanowires, nanobeams, and ultrathin films are excellent platforms for the exploration of flexoelectric effects.

Research trends and emerging fields of interest

Over the past two decades, flexoelectricity has evolved from a theoretical concept into a rapidly growing field of research. A bibliometric analysis of the Web of Science database using the keyword "flexoelectricity" clearly illustrates this trend [Figure 3], with the number of publications having grown considerably since the early 2000s, marked by notable increases after 2010 as experimental techniques matured. Early studies focused on measuring coefficients and validating theoretical models, whereas recent works have increasingly highlighted the functional applications of flexoelectricity, including energy harvesting, photocatalysis, and domain engineering[25,31,32].

This growing interest is also reflected in the diversity of research topics. Flexoelectricity is now investigated not only in perovskite oxides but also in layered oxides, multiferroics, and metallic oxides, where unconventional polar responses have been reported. The field has thus expanded beyond fundamental characterization to include device-oriented studies, theoretical simulations, and coupling phenomena with other orders such as magnetism and metallicity[17].

In the following sections, we focus on how flexoelectricity in oxides can be deliberately induced and exploited through strain, electric-field, and chemical gradient engineering. Representative material systems and associated functionalities, including flexo-photovoltaic effects, catalytic enhancement, polarization switching and domain tailoring, flexoelectronic device concepts, the control of magnetism and spin textures, polarization gradients, large built-in-fields, the novel control of domain structures, and piezoelectric/pyroelectric responses, are then described to highlight the fundamentals and practical design principles of flexoelectricity in functional oxide materials.

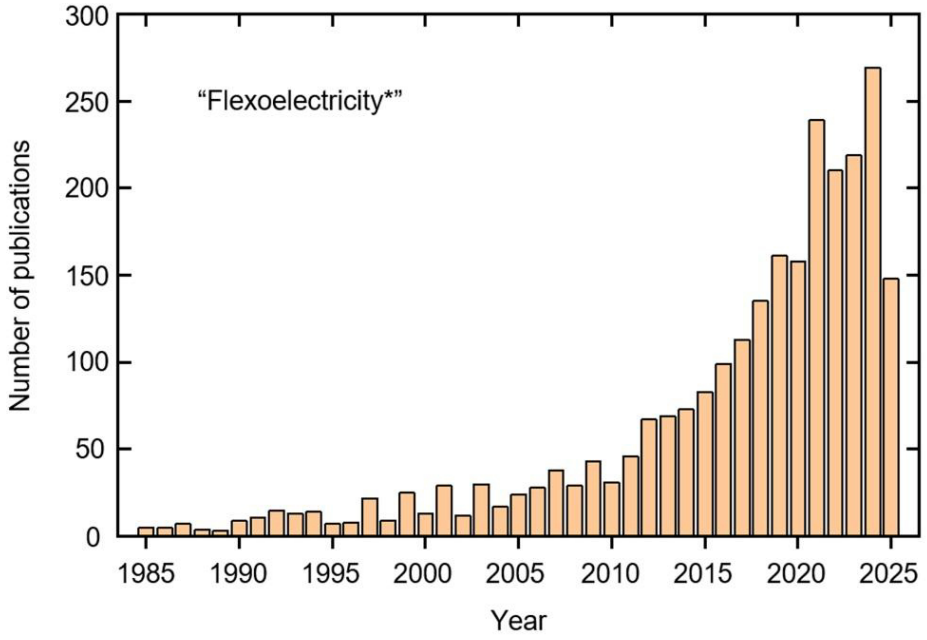

Figure 3. Number of publications related to flexoelectricity retrieved from the Web of Science database (keyword search: "flexoelectricity*") between 1985 and 2025.

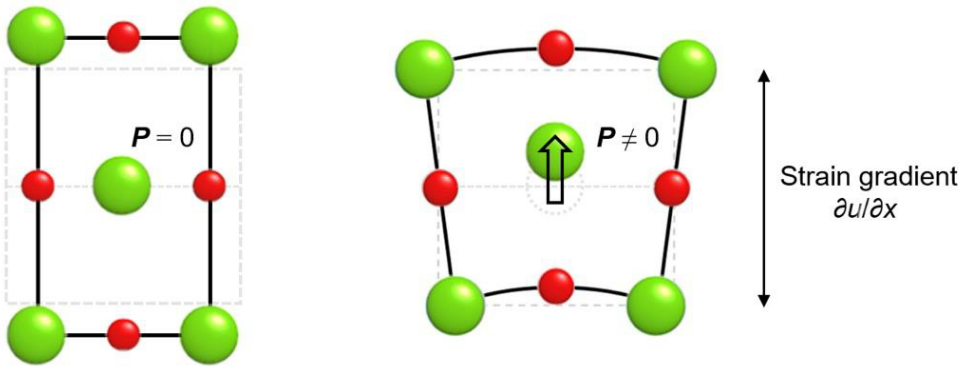

Figure 4. Schematic illustration of strain gradient formation. Homogeneous compression or tension with no net polarization (left) and bending deformation with a strain gradient and induced polarization (right) are illustrated.

STRAIN GRADIENT ENGINEERING

Strain gradients and flexoelectricity

A strain gradient is characterized by the spatial variation of strain within a material, denoted as $\partial u/\partial x$, where u is the displacement and x is the position. Unlike uniform strain, which applies homogeneous deformation and preserves inversion symmetry, a strain gradient produces asymmetric distortions that locally disrupt this symmetry, inducing polarization through the flexoelectric effect. This distinction is clearly illustrated in Figure 4. Under uniform compression or tension, centrosymmetric materials remain nonpolar ($P = 0$). In contrast, bending a crystal produces tensile strain on one side and compressive strain on the other, generating a continuous strain gradient across the thickness. This imbalance results in a finite polarization ($P \neq 0$), even though the bulk material is centrosymmetric.

As discussed earlier, this phenomenon is formally captured using the flexoelectric constitutive relation, in which polarization is proportional to the strain gradient via the flexoelectric tensor. Thus, flexoelectricity

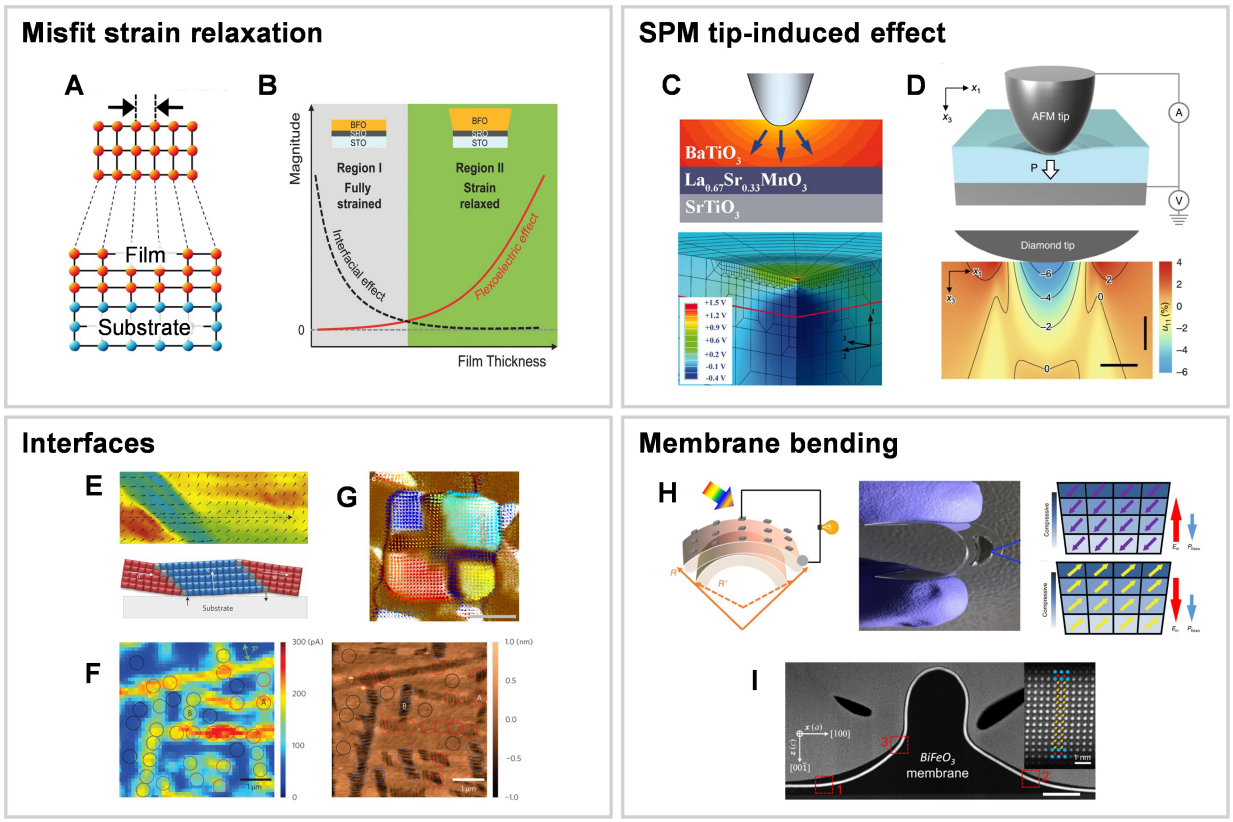

Figure 5. Representative methods for generating strain gradients in oxide materials. (A and B) Misfit strain relaxation in epitaxial thin films. (A) Schematic illustration of strain relaxation in $HoMnO_3$ thin films. Reproduced with permission[6]. Copyright 2011, American Physical Society. (B) Relaxation behavior of $BiFeO_3$ epitaxial films. Reproduced with permission[54]. Copyright 2013, John Wiley and Sons; (C and D) SPM-tip-induced flexoelectric effects. (C) Schematic illustration of AFM-tip loading on a $BaTiO_3/La_{0.67}Sr_{0.33}MnO_3$ heterostructure. Reproduced with permission[25]. Copyright 2012, American Association for the Advancement of Science. (D) Schematic and phase-field simulation of ultrathin $SrTiO_3$ under AFM-tip loading. Reproduced with permission[33]. Copyright 2020, Springer Nature; (E-G) Interfacial strain gradients in oxide heterostructures and multilayers. (E) Strain and polarization mapping of a-c domain films with corresponding schematic. Reproduced with permission[21]. Copyright 2011, Springer Nature. (F) Photocurrent mapping and surface morphology of mixed-phase regions. Reproduced with permission[20]. Copyright 2015, Springer Nature. (G) In-plane piezoresponse vector mapping of strain-graded ferroelectric nanoplates. Reproduced with permission[59]. Copyright 2018, Springer Nature; (H and I) Bending of freestanding membranes. (H) Schematic and optical images of bent $BiFeO_3$ membranes. Reproduced with permission[29]. Copyright 2020, Springer Nature. (I) Cross-sectional STEM image of a wrinkled freestanding $BiFeO_3$ membrane. Reproduced with permission[43]. Copyright 2022, Springer Nature. SPM: Scanning probe microscopy; AFM: atomic force microscopy; STEM: scanning transmission electron microscopy; BFO: $BiFeO_3$; SRO: $SrRuO_3$; STO: $SrTiO_3$.

depends on the gradient of the strain rather than the strain itself, fundamentally distinguishing it from piezoelectricity.

Methods for generating strain gradients

Strain gradients in complex oxides can arise from lattice mismatches, dislocations, or interfacial distortions, and can also be externally imposed using local probes or mechanical bending. These approaches can produce controlled strain gradient profiles and tunable flexoelectric polarization. Figure 5 summarizes representative strategies, including misfit strain relaxation, SPM tip-induced deformation, interfacial engineering, and membrane bending, each offering distinct advantages in terms of scalability, spatial precision, and coupling to other functional responses. In the following subsections, we discuss these approaches in detail.

Misfit strain relaxation

In epitaxial thin films, a lattice mismatch between the film and substrate generates strain at the interface. This strain is not uniform but gradually relaxes away from the interface, leading to a vertical strain gradient

across the film thickness. In perovskite oxides, significant lattice mismatches can be accommodated, thus misfit-driven relaxation processes represent a natural source of strong strain gradients and consequently flexoelectric polarization[6,54-57].

The degree of strain relaxation can be effectively tuned by controlling the growth conditions. Lee *et al.* demonstrated that adjusting the oxygen partial pressure during deposition significantly modifies strain relaxation, enabling the incorporation of extremely large strain gradients on the order of 10^5-10^6 m^{-1} into ferroelectric thin films [Figure 5A][6]. Building on this concept, Jeon *et al.* investigated epitaxial $BiFeO_3$ thin films and showed that both deposition temperature and film thickness are decisive factors in strain relaxation[54]. Their results revealed that self-polarization arises from the competition between interfacial effects and flexoelectric contributions, and that this balance can be shifted by reducing the growth temperature or adjusting the thickness of the film. Consequently, the direction of the self-poling effect in $BiFeO_3$ films can be deliberately reversed [Figure 5B]. Similar behavior has also been observed in $BaTiO_3$ thin films[55]. These built-in gradients generate strong internal fields that align dipole defects during cooling, thus modifying the domain configurations and altering polarization-electric field hysteresis loops[6,56]. Moreover, when combined with thickness control, this strain gradient-induced polarization has been linked to rectifying diode-like behavior in ferroelectric films, demonstrating that misfit strain relaxation is both a robust source of polarization and a pathway to emergent electronic functionalities[54,56,57].

SPM tip-induced effects

SPM is a versatile platform for the generation of localized strain gradients in oxide thin films. Mechanical indentation using a sharp tip produces strongly inhomogeneous lattice deformation and steep nanoscale strain gradients beneath the tip, inducing flexoelectric polarization. This high degree of spatial localization enables the direct observation and manipulation of flexoelectric effects at a nanoscale resolution.

In an early demonstration, Lu *et al.* applied an atomic force microscopy (AFM)-based mechanical loading to ferroelectric thin films and reported that tip-induced strain gradients strongly influence domain stability and evolution [Figure 5C][25]. Their work demonstrated that local mechanical perturbations could significantly alter polarization behavior through flexoelectric coupling. Later work by Park *et al.* investigated epitaxial $SrTiO_3$ thin films and revealed that nanoscale indentation with an AFM tip can generate measurable polarization in a material that is otherwise centrosymmetric and nonpolar in its bulk form [Figure 5D][33]. Their study provided direct evidence that strain gradients alone can locally break inversion symmetry and activate polarization in non-ferroelectric oxides.

Collectively, these results establish SPM indentation as a robust method for the probing and manipulation of flexoelectric coupling at the nanoscale. In addition to fundamental studies, tip-induced strain gradients also have the potential to generate device-relevant functionalities in oxide thin films, where polarization states can be locally engineered at a high spatial resolution[32,58].

Interfacial effects

Interfacial effects in complex oxide heterostructures and multilayers can also generate strain gradients. When two dissimilar materials are joined, differences in their lattice parameters, symmetry, or ferroic ordering create inhomogeneous strain fields near the interface. These distortions often extend several nanometers into the adjacent layers, establishing gradients that strongly couple to polarization and other order parameters.

One of the first reports of interfacial strain gradient-driven polarization came from Catalan *et al.*, who showed that asymmetric interfacial strain relaxation in $PbTiO_3$ films produces vertical and lateral strain gradients that rotate the spontaneous polarization, providing clear evidence of interfacial strain gradient

polarization engineering in ferroelectric oxide films [Figure 5E][21]. Chu *et al.* subsequently reported that large interfacial strain gradients at the polymorphic phase boundaries in $BiFeO_3$ give rise to pronounced photoresponse anisotropy, i.e., the flexo-photovoltaic enhancement of the photocurrent localized near the interface [Figure 5F][20]. This established a direct link between interfacial strain gradients and optoelectronic functionality. More recently, Kim *et al.* reported that strain gradients in ferroelectric epitaxial thin films can stabilize unusual topological domain textures such as vortices and antivortices [Figure 5G][59]. This flexoelectricity-driven polarization rotation is particularly noteworthy because polarization rotation is widely regarded as a key mechanism underlying enhanced piezoelectric responses. These findings therefore suggest potential strategies for realizing large electromechanical effects in lead-free ferroelectric systems.

Membrane bending

The geometry of freestanding oxide membranes and nanobeams is conducive to the development of well-defined strain gradients. In contrast to epitaxial thin films clamped to rigid substrates, these membranes are mechanically free, meaning that bending produces a highly uniform tensile strain on one side and compressive strain on the other, resulting in a large and controllable strain gradient across the thickness. These systems thus provide a versatile experimental platform for the analysis of flexoelectricity under macroscopic bending deformation.

In a representative example, bending-induced strain gradients in $BiFeO_3$ membranes were demonstrated by Guo *et al.* to generate macroscopic flexoelectric fields capable of continuously tuning photoconductance [Figure 5H][29]. By systematically adjusting the bending curvature, the photocurrent response could be tuned in a nearly linear and reversible manner, without the need for external bias or compositional modifications. These results demonstrate that flexoelectricity can serve as an intrinsic mechanism for dynamic optoelectronic control. More recently, Cai *et al.* investigated freestanding perovskite oxide membranes and found that bending not only amplified the net polarization but also produced abnormal flexural deformation beyond classical elastic expectations [Figure 5I][43]. These observations suggest that strain gradients strongly influence both electrical and mechanical responses, reinforcing the view that flexoelectricity in membrane systems can unlock functionalities that cannot be obtained in bulk materials or clamped films.

Applications of strain gradients and flexoelectricity

Flexo-photovoltaic effects

The coupling of strain gradients with light-matter interactions has opened new research directions that combine electromechanics and optoelectronics. An example of this is the flexo-photovoltaic effect, which describes the generation or modulation of photocurrent by strain gradient-induced polarization fields, even in materials that lack spontaneous polarization. This concept expands the scope of photovoltaic phenomena while representing a versatile means to control carrier dynamics via structural engineering.

An early experimental indication of strain gradient-driven photovoltaic behavior was reported by Chu *et al.*, who investigated epitaxial $BiFeO_3$ thin films containing polymorphic phase boundaries[20]. At these boundaries between tetragonal-like and rhombohedral-like regions, extremely large strain gradients were observed, reaching values of approximately 3.3×10^7 m^{-1}. These gradients generated strong internal flexoelectric fields capable of influencing carrier dynamics. Spatially resolved photocurrent mapping revealed that the most intense anisotropic photocurrent signals were localized at these boundary regions [Figure 6A-C], establishing a direct correlation between large strain gradients and enhanced charge separation in complex oxide thin films.

While Chu *et al.* demonstrated that strain gradient-driven photovoltaic responses can originate from strain gradients that naturally form at polymorphic phase boundaries in $BiFeO_3$ thin films[20], Guo *et al.* investigated

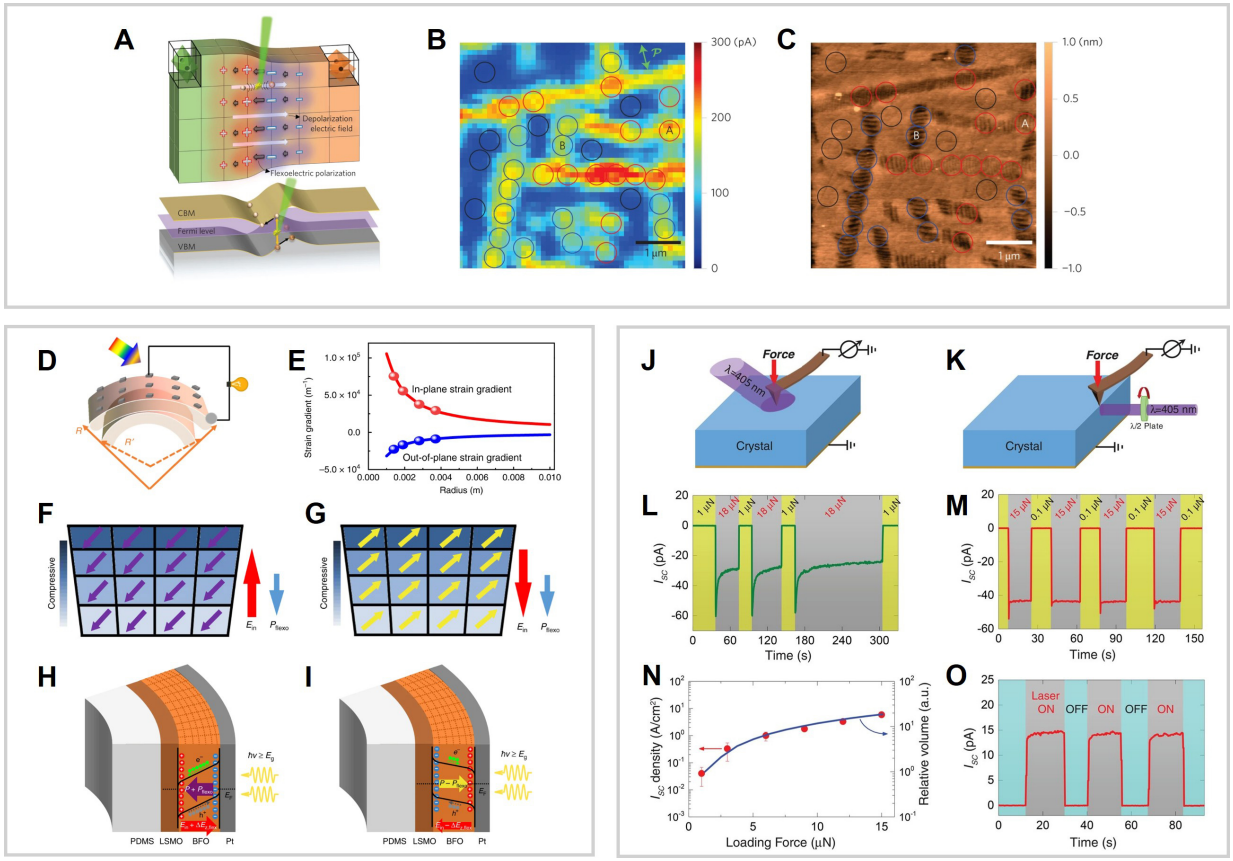

Figure 6. Flexoelectricity-driven photovoltaic effects in oxides and crystals. (A) Schematic illustration of flexoelectric polarization at polymorphic phase boundaries in $BiFeO_3$ thin films. (B) Conductive AFM photocurrent mapping of phase boundaries. (C) PFM phase image of $BiFeO_3$ thin films showing polymorphic domain structures. (A-C) Reproduced with permission[20]. Copyright 2015, Springer Nature; (D) Schematic illustration of bending-induced strain gradients in freestanding membranes. (E) Calculated strain distribution during bending. (F and G) Schematics of polarization and flexoelectric fields in (F) downward- and (G) upward-polarized $BiFeO_3$ membranes under bending; (H and I) Band diagrams of bent $BiFeO_3$ membranes in (H) downward- and (I) upward-polarized states. (D-I) Reproduced with permission[29]. Copyright 2020, Springer Nature; (J) Schematic of the experimental setup for flexo-photovoltaic measurements using AFM-tip loading. (K) Side-illumination geometry for photocurrent measurements. (L) Photocurrent collected by a conductive AFM tip under a high loading force on the $SrTiO_3$ (001) surface. (M) Photocurrent response on the TiO_2 (100) surface under a tip loading force. (N) Dependence of the short-circuit current on the applied loading force. (O) Photocurrent modulation under on/off laser illumination. (J-O) Reproduced with permission[30]. Copyright 2018, American Association for the Advancement of Science. AFM: Atomic force microscopy; PFM: piezoresponse force microscopy; LSMO: $La_{0.67}Sr_{0.33}MnO_3$; BFO: $BiFeO_3$; PDMS: polydimethylsiloxane.

the same material as a freestanding membrane, with this distinct geometry used to deliberately impose macroscopic strain gradients[29]. This approach provided an externally controllable means to study the effect, complementing the boundary-driven mechanism observed in thin films and offering a pathway to mechanically tunable optoelectronics.

In later research, Guo *et al.* showed that bending freestanding $BiFeO_3$ membranes induces macroscopic strain gradients that are capable of continuously regulating photoconductance[29]. A flexible Pt/$BiFeO_3$/$La_{0.67}Sr_{0.33}MnO_3$ (LSMO) device was realized by transferring the heterostructure onto a polydimethylsiloxane (PDMS) support [Figure 6D]. In this device, the bending radius R defined the magnitude of the strain gradient in the membrane, with smaller radii corresponding to stronger gradients [Figure 6E]. Under upward bending, asymmetric lattice distortions produced regions with distinct polarization orientations [Figure 6F and G]. The resulting flexoelectric field coupled with the intrinsic polarization-dependent field (E_{in}), thus modulating the photocurrent and photovoltage in a reversible manner. The observation that bending directly altered the photoconductance confirmed the active role of

flexoelectricity in the photovoltaic response of freestanding $BiFeO_3$. To interpret this behavior, schematic band diagrams were produced [Figure 6H and I], showing that, when $BiFeO_3$ polarization was oriented upward, the flexoelectric contribution acted in the opposite direction, partially compensating E_{in} and reducing the carrier separation efficiency. In contrast, when the polarization was oriented downward, the flexoelectric field reinforced E_{in}, leading to steeper band bending and enhanced charge separation. This bidirectional tunability demonstrates that strain gradients can be harnessed to achieve multilevel conductance states in flexible oxide devices, establishing bending control as a practical strategy for tailoring the optoelectronic performance of ferroelectric membranes and paving the way for the development of mechanically reconfigurable photovoltaics.

In addition to polymorphic phase boundaries within $BiFeO_3$ thin films and bending-induced gradients in freestanding membranes, strain gradients and their associated photovoltaic responses can also be realized using scanning probes. Yang *et al.* demonstrated that controlled indentation with a scanning probe tip can impose large local strain gradients, with the resulting flexoelectric polarization directly modulating the photovoltaic effect in $SrTiO_3$ and TiO_2 single crystals[30]. In their photoelectric AFM configuration [Figure 6J and K], a conductive tip applied local forces on the crystal surface while simultaneously collecting the photocurrent. Under illumination, the short-circuit current was strongly dependent on the applied load, with an increase in the force from 1 mN to 18 mN enhancing the photocurrent density by more than two orders of magnitude [Figure 6L-N]. Current densities up to ~1 A cm^{-2} were recorded within the nanoscale contact area, far exceeding those of conventional Schottky junctions under similar conditions. This response was also stable under sustained loading and reversible with repeated light cycling [Figure 6O], providing compelling evidence that strain gradient-induced flexoelectric polarization can produce a robust photovoltaic effect even in centrosymmetric oxides, where conventional bulk photovoltaic effects are symmetry-forbidden.

Collectively, these studies establish flexo-photovoltaics as a versatile and broadly applicable mechanism for light-to-electricity conversion. By demonstrating that strain gradients, whether they are naturally occurring at phase boundaries, mechanically imposed in membranes, or locally generated via scanning probe indentation, can generate or modulate a photocurrent, they extend the photovoltaic paradigm beyond ferroelectric materials. This strong association between mechanical deformation and the photoresponse means that flexoelectricity has the potential to play a significant role in the development of reconfigurable, highly efficient, and multifunctional optoelectronic devices.

Catalysts

The recent combination of strain gradient engineering with catalysis has opened new opportunities because flexoelectric polarization can directly modulate surface charge distribution and adsorption energetics. This provides a new strategy to enhance photocatalytic, piezocatalytic, and electrocatalytic activities in complex oxides and related materials.

Ultrasonication has proven to be a versatile method for the generation of strain gradients and activation of flexoelectric polarization for catalysis. Cheng *et al.* systematically examined this approach in centrosymmetric Ag_2MoO_4 particles, comparing photocatalysis under simulated sunlight, flexocatalysis under ultrasonic vibration, and flexo-photocatalysis under simultaneous excitation[60]. Flexo-photocatalysis produced the strongest performance, with methylene blue degradation rates that were 1.88- and 23.07-fold higher than photocatalysis and flexocatalysis alone, respectively [Figure 7A and B]. This enhancement was attributed to ultrasound-induced strain gradients generating polarization fields that promoted charge separation and accelerated activity.

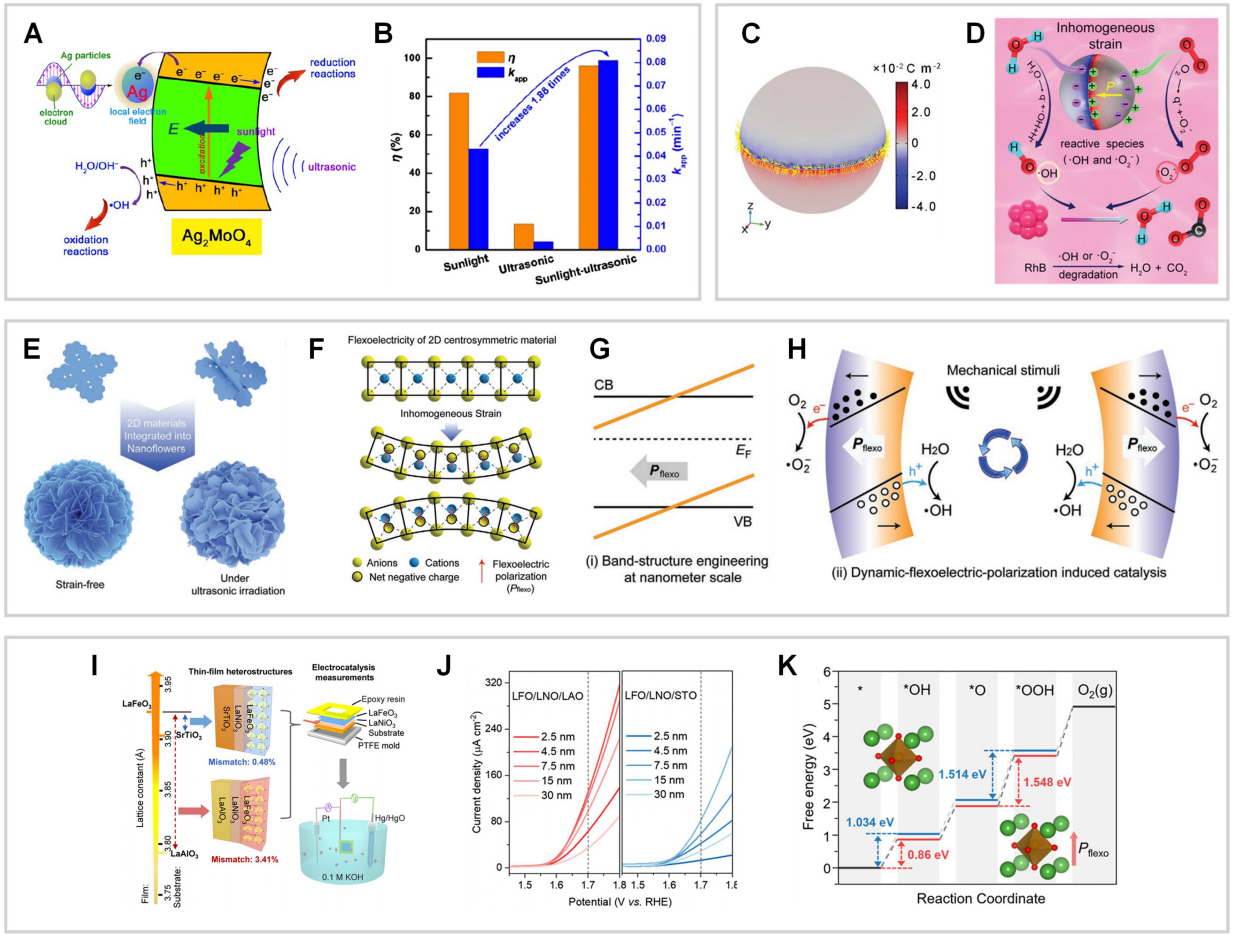

Figure 7. Flexoelectricity-enhanced catalytic activity in oxides and thin films. (A) Schematic of photocatalysis, flexocatalysis, and flexo-photocatalysis in centrosymmetric Ag_2MoO_4 under simulated sunlight and ultrasonic vibration. (B) Photocatalytic efficiency for methylene blue degradation under photocatalysis, flexocatalysis, and flexo-photocatalysis. (A and B) Reproduced with permission[60]. Copyright 2021, Elsevier; (C) Finite-element modeling of the strain distribution generated by ultrasound-induced bubble cavitation in $SrTiO_3$ nanoparticles. (D) Schematic of reactive oxygen species generation associated with flexoelectric polarization under inhomogeneous strain. (C and D) Reproduced with permission[61]. Copyright 2022, John Wiley and Sons; (E) Morphology of MnO_2 nanoflowers composed of 2D nanosheets before and after ultrasonication. (F) Illustration of flexoelectric polarization in 2D centrosymmetric MnO_2 under inhomogeneous strain. (G) Band-structure modulation by flexoelectric polarization. (H) Schematic of catalytic reactions under dynamic flexoelectric polarization. (E-H) Reproduced with permission[62]. Copyright 2023, John Wiley and Sons; (I) Strain gradient engineering in $LaFeO_3$ thin films grown on $LaNiO_3/LaAlO_3$ and $LaNiO_3/SrTiO_3$ substrates. (J) Linear sweep voltammetry of $LaFeO_3$ heterostructures for the oxygen evolution reaction (OER). (K) Gibbs free-energy calculations for the OER steps. (I-K) Reproduced with permission[31]. Copyright 2024, AIP Publishing. 2D: Two-dimensional; RHE: reversible hydrogen electrode; LFO: $LaFeO_3$; LNO: $LaNiO_3$; LAO: $LaAlO_3$.

Building on this, Liu *et al.* investigated centrosymmetric $SrTiO_3$ nanoparticles in which ultrasound-induced bubble cavitation produced localized strain gradients as large as 2.7×10^6 m^{-1}, far exceeding those typically obtained in macroscopic bending experiments[61]. These gradients induced flexoelectric polarization that cyclically generated reactive oxygen species (·OH, ·O_2^-), leading to efficient pollutant degradation. $SrTiO_3$ nanoparticles achieved a reaction rate constant of ~0.6 h^{-1} and degraded more than 92% of Rhodamine B, confirming the catalytic efficacy of cavitation-driven flexoelectricity [Figure 7C and D]. The approach has been extended to TiO_2 and mica, highlighting its utility with various centrosymmetric oxides.

More recently, Wu *et al.* expanded the concept to 2D semiconductors, reporting the first flexocatalysis in MnO_2 nanosheet-assembled nanoflowers[62]. Under ultrasonic simulation, the nanoflower morphology promoted the generation of strong nanoscale inhomogeneous strain profiles, leading to dynamic flexoelectric

polarization [Figure 7E and F]. These fields acted as an internal driving force for band-structure modulation [Figure 7G] and sustained redox reactions [Figure 7H]. As a result, organic pollutants such as methylene blue could be degraded within 5 min, with a performance comparable to state-of-the-art piezocatalysis while maintaining excellent stability and reproducibility. Wu *et al*. also examined the effects of factors such as the morphology, absorption, vibration intensity, and temperature, producing stronger mechanistic insights into flexocatalysis in 2D systems[62].

These studies have established ultrasonication as a general and scalable route for the activation of flexoelectric polarization for catalysis. Progressing from bulk oxides to nanoparticles and ultimately to 2D semiconductors, ultrasound-driven flexocatalysis represents a powerful platform for environmental purification and a promising extension of flexoelectricity into electrochemical functionalities.

In contrast to these ultrasound-driven approaches, Xu *et al*. recently demonstrated that flexoelectricity can be harnessed in epitaxial thin-film heterostructures to enhance electrocatalytic water splitting[31]. In their work, $LaFeO_3$ thin films were grown on $LaNiO_3$-buffered $SrTiO_3$ and $LaAlO_3$ substrates. Because the lattice mismatch between $LaFeO_3$ and $SrTiO_3$ was relatively small, strain relaxation did not generate significant strain gradients, thus flexoelectric polarization was negligible. In contrast, the larger mismatch with $LaAlO_3$ induced pronounced strain relaxation, leading to strong strain gradients and measurable flexoelectric polarization [Figure 7I]. Electrochemical testing revealed that both systems had similar onset potentials of ~1.57 V versus the reversible hydrogen electrode (RHE), but the $LaFeO_3/LaNiO_3/LaAlO_3$ films exhibited a much steeper rise in the current density, leading to a ~300% enhancement in oxygen evolution reaction (OER) activity relative to the $SrTiO_3$-based heterostructure [Figure 7J]. Density functional theory and Gibbs free-energy calculations further showed that, while later OER steps (*OOH formation) remained comparable, a key difference was observed in step 1 (*OH formation). Here, the energy barrier was reduced by 0.174 eV in the $LaAlO_3$-based system, a consequence of flexoelectric band bending that strengthened hydroxy absorption and accelerated electron transfer across the catalyst-electrolyte interface [Figure 7K]. These findings demonstrate that substrate-controlled strain relaxation can introduce flexoelectric polarization that is absent in $SrTiO_3$-based films, directly improving OER activity. This static, strain gradient-driven approach complements ultrasound-based flexocatalysis, highlighting flexoelectricity as a versatile strategy for catalytic enhancement in both environmental and energy applications.

Polarization switching and domain tailoring

The control of ferroelectric polarization through strain gradients is one of the most compelling demonstrations of flexoelectricity in functional oxides because it provides a purely mechanical alternative to conventional electric-field-driven switching. Straightforward mechanical estimations suggest that applying only a few micronewtons of force through a sharp AFM tip can generate localized stresses of several gigapascals, which decay within tens of nanometers from the contact center. This intense stress field couples directly to the ferroelectric order parameter via piezoelectric and flexoelectric interactions. In ultrathin ferroelectric films, this coupling lowers the coercive field, leading to polarization switching under purely mechanical loading conditions.

Building on this concept, Lu *et al*. performed a pioneering experiment on epitaxial $BaTiO_3$ thin films, demonstrating that AFM tip-induced strain gradients can mechanically write and erase ferroelectric domains without an external electric field[25]. By applying only a few micronewtons of force, they showed deterministic polarization reversal and nanoscale domain patterning, providing the first direct evidence that the flexoelectric fields generated by strain gradients are sufficient to overcome the coercive barrier [Figure 8A and B]. This established the "mechanical writing" of ferroelectricity and its potential for nanoscale data storage and domain engineering [Figure 8C and D].

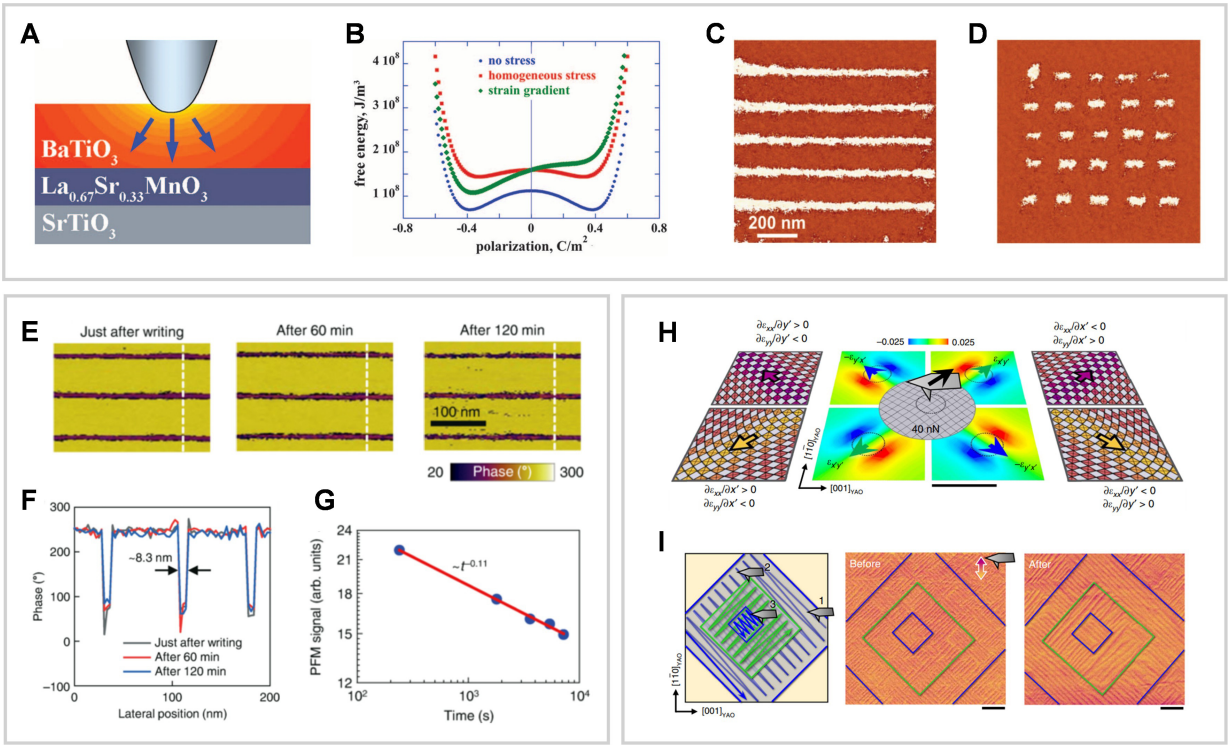

Figure 8. Flexoelectricity-driven polarization switching and domain tailoring in ferroelectrics. (A) Schematic illustration of AFM-tip-induced strain gradients in epitaxial $BaTiO_3$ thin films. (B) Free-energy landscape under a strain gradient. (C and D) AFM writing experiments for (C) creation and (D) erasure of nanoscale domain patterns using only mechanical force. (A-D) Reproduced with permission[25]. Copyright 2012, American Association for the Advancement of Science; (E) Domain evolution in metastable $CaTiO_3$ after mechanical writing at an ultralow force (~100 nN). (F and G) PFM signal analysis of domain stability and storage density. (F) Cross-sectional PFM phase profiles measured after 120 min. (G) Time-dependent PFM amplitude as a function of time. (E-G) Reproduced with permission[67]. Copyright 2022, American Physical Society; (H) Atomic-resolution strain mapping at ferroelastic twin walls in WO_3 films. (I) Scanning-tip-controlled reorientation of ferroelastic walls. (H and I) Reproduced with permission[32]. Copyright 2020, Springer Nature. AFM: Atomic force microscopy; PFM: piezoresponse force microscopy.

Following this initial discovery, similar forms of mechanically induced polarization control have been reproduced in a wide range of ferroelectrics, including $BaTiO_3$ thin films with top electrodes[63], $PbTiO_3$[64], nanopolar regions in $SrTiO_3$[65], and multiferroics such as $BiFeO_3$[58] and $TbMnO_3$[66]. These studies have confirmed that flexoelectricty-driven polarization switching is not confined to a single material system but can be broadly applied to various materials, including perovskite oxides and multiferroics.

Lee *et al*. later extended this approach to metastable $CaTiO_3$ ferroelectrics, where the intrinsically low coercivity enabled highly efficient switching under forces as small as ~100 nN[67]. This allowed the creation of sub-10 nm domains, corresponding to an ultrahigh potential storage density of ≥ 1 Tbit cm^{-2} [Figure 8E-G]. Their results demonstrated that flexoelectricity-driven mechanical switching is both feasible and scalable for high-density data-storage technologies.

Flexoelectricity has also been observed in WO_3 thin films, with the ferroelastic domain walls acting as functional sites. Yun *et al*. reported that ferroelastic twin walls in centrosymmetric WO_3 exhibit exceptionally large strain gradients of ~10^6 m^{-1} across widths of ~20 nm[32]. This led to enhanced piezoelectric-like behavior, referred to as flexopiezoelectricity, despite the bulk being non-polar. Atomic-resolution scanning transmission electron microscopy (STEM) confirmed lattice distortions, while differential phase-contrast imaging visualized the associated depolarized fields [Figure 8H]. The extracted flexopiezoelectric coefficient (~30 J C^{-1}) and lateral piezoresponse amplitude (~6 pm V^{-1}) quantitatively established the strength of this

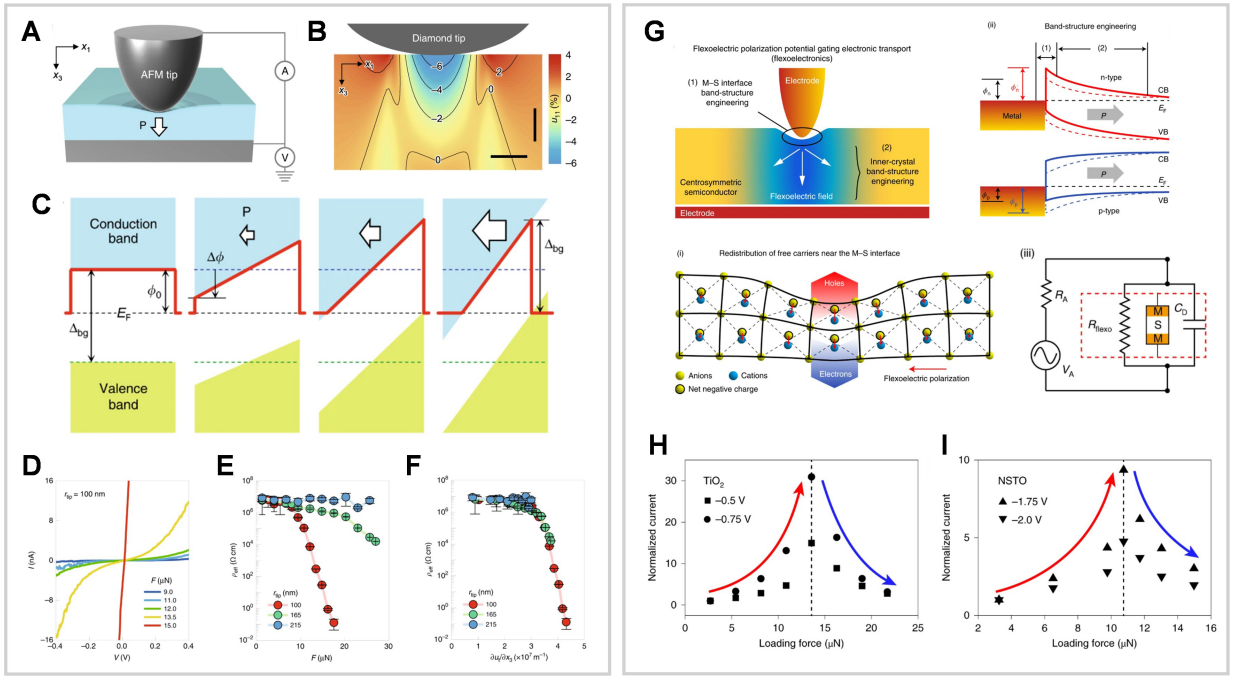

Figure 9. Flexoelectronics enabled by strain gradient-induced polarization. (A and B) (A) Schematic and (B) finite-element simulation of an AFM-tip-induced strain gradient in ultrathin $SrTiO_3$ films; (C) Band-structure evolution under increasing flexoelectric fields; (D-F) Colossal flexoresistance in $SrTiO_3$: (D) I-V curves under varying loading forces, (E) effective resistivity (ρ_{eff}) as a function of the tip force, and (F) ρ_{eff} as a function of strain gradient. (A-F) Reproduced with permission[33]. Copyright 2019, Springer Nature; (G) Concept of flexoelectronics in centrosymmetric semiconductors at a metal-semiconductor interface. (H and I) Experimental flexoelectronic transport measurements in (H) TiO_2 and (I) Nb-doped $SrTiO_3$ under strain gradients. (G-I) Reproduced with permission[9]. Copyright 2020, Springer Nature. AFM: Atomic force microscopy; CB: conduction band; VB: valence band.

effect. These ferroelastic walls could also be manipulated deterministically using scanning probe-induced stress, which reoriented and aligned the domain-wall configuration [Figure 8I]. This demonstrated that shear strain gradients at ferroelastic walls are active flexoelectric sources, providing the opportunity for domain-wall-based electromechanical functionalities and nanoscale actuation.

Flexoelectronics

Flexoelectronics has expanded strain gradient engineering into electronic transport, offering a universal mechanism for the modulation of conductivity in materials that are otherwise insensitive to conventional polarization engineering. By exploiting the coupling between mechanical strain gradients and internal polarization potentials, flexoelectronics provides a pathway to overcome the inability of dielectrics and semiconductors to reversibly switch electronic states[68] without a catastrophic breakdown[69].

Park *et al.* investigated this phenomenon in ultrathin $SrTiO_3$ films, where local strain gradients were generated using an AFM tip [Figure 9A and B][33]. The intense nanoscale fields induced by flexoelectric polarization modified the electronic band landscape, progressively reducing the effective tunnel barrier height and eventually driving the conduction and valence bands to cross the Fermi level [Figure 9C]. This crossing promoted the Zener breakdown[70], producing an abrupt insulator-to-conductor transition. Conductive AFM measurements revealed a dramatic drop in the resistivity of nearly 10^8-fold at room temperature, with clear load-dependent behavior [Figure 9D-F]. This colossal flexoresistance effect was reversible; once the applied force was removed, the $SrTiO_3$ films recovered their insulating properties without structural degradation. These findings demonstrate that flexoelectricity is a nondestructive method for applying extremely strong internal electrostatic fields in dielectrics, enabling a form of electronic-state switching that had long been thought unattainable.

Wang *et al.* broadened this framework by demonstrating the flexoelectronic effect in a wide range of centrosymmetric semiconductors, including Si, TiO_2, and Nb-doped $SrTiO_3$[9]. In this approach, the flexoelectric polarization field acted as an internal gate, modulating the Schottky barrier height at the metal-semiconductor interface [Figure 9G]. Redistribution of free carriers near the interface directly altered charge transport, effectively allowing mechanical control of electronic states; this was demonstrated in TiO_2 and Nb-doped $SrTiO_3$, where the AFM tip loading modulated the current response [Figure 9H and I]. Strain sensitivities exceeding 2,650 were reported, alongside ultrafast response times (< 4 ms) and a spatial resolution down to ~0.78 nm. These performance metrics were a substantial improvement on those achieved by state-of-the-art Si nanowire strain sensors, as well as piezoresistive and ferroelectric devices[71].

Collectively, these results establish flexoelectronics as a generalizable approach for mechanically tuning conductivity in both dielectric and semiconductors. By coupling strain gradients to polarization potentials, flexoelectric fields enable the reversible, high-resolution, and ultrafast modulation of electronic transport for potential use in mechanically gated transistors, ultrasensitive strain sensors, and multifunctional electromechanical devices.

Control of magnetism or spin texture

The exploration of flexoelectricity in magnetic systems has recently uncovered new strategies to manipulate spin order, magnetic phase transitions, and spin textures through strain gradients[72]. These advances are particularly significant because they provide mechanical pathways to engineer the Dzyaloshinskii-Moriya interaction (DMI)[34,73,74], Néel temperature distribution[75], emergent polar-magnetic coupling[17,35,76], and momentum-space spin textures[77], phenomena that were previously thought to require non-centrosymmetric lattices or strong external fields.

Zhang *et al.* demonstrated that graded strain can stabilize room-temperature magnetic skyrmions in the centrosymmetric manganite LSMO[34]. Using epitaxial growth on a $NdGaO_3$ substrate, their study engineered tensile strain relaxation across the film thickness, generating strain gradients on the order of 10^5 m^{-1} [Figure 10A and B]. This gradient broke inversion symmetry and induced an emergent DMI containing both helicoid- and cycloid-type components. As a result, robust zero-field skyrmion lattices (~120 nm diameter) and spin spirals (periodicity ~150 nm) were observed at 300 K [Figure 10C][34]. Magnetotransport measurements revealed topological Hall effect signatures, confirming their nontrivial topology. These findings establish strain engineering as a viable route to stabilize chiral spin textures in correlated centrosymmetric oxides.

Makushko *et al.* extended the scope of strain-gradient control of magnetism to antiferromagnetic insulators by investigating Cr_2O_3 thin films under strain gradients[75]. They observed a vertical distribution of the Néel temperature ranging from ~60 ℃ near the interface to ~100 ℃ at the surface of 50-nm-thick films [Figure 10D and E]. This inhomogeneous transition was quantified with a flexomagnetic coefficient of ~15 μB nm^{-2}, providing direct evidence for the strain gradient-driven modulation of the antiferromagnetic order. This study demonstrates that spatial gradients in structural parameters can be employed to control spin superfluidity, magnonic excitation, and soliton dynamics, thus offering useful design rules for reconfigurable spintronic devices[78].

A complementary manifestation of symmetry engineering was reported by Liu *et al.*, who introduced strain gradients to Sr_2IrO_4, a centrosymmetric spin-orbit coupled antiferromagnet[35]. Breaking inversion symmetry through nonequivalent O p-Ir d hybridization along the out-of-plane direction resulted in the simultaneous emergence of a polar phase and an unconventional z-axis magnetic moment [Figure 10F]. The flexomagnetoelectric coupling was confirmed by the ability to tune polarization through external magnetic

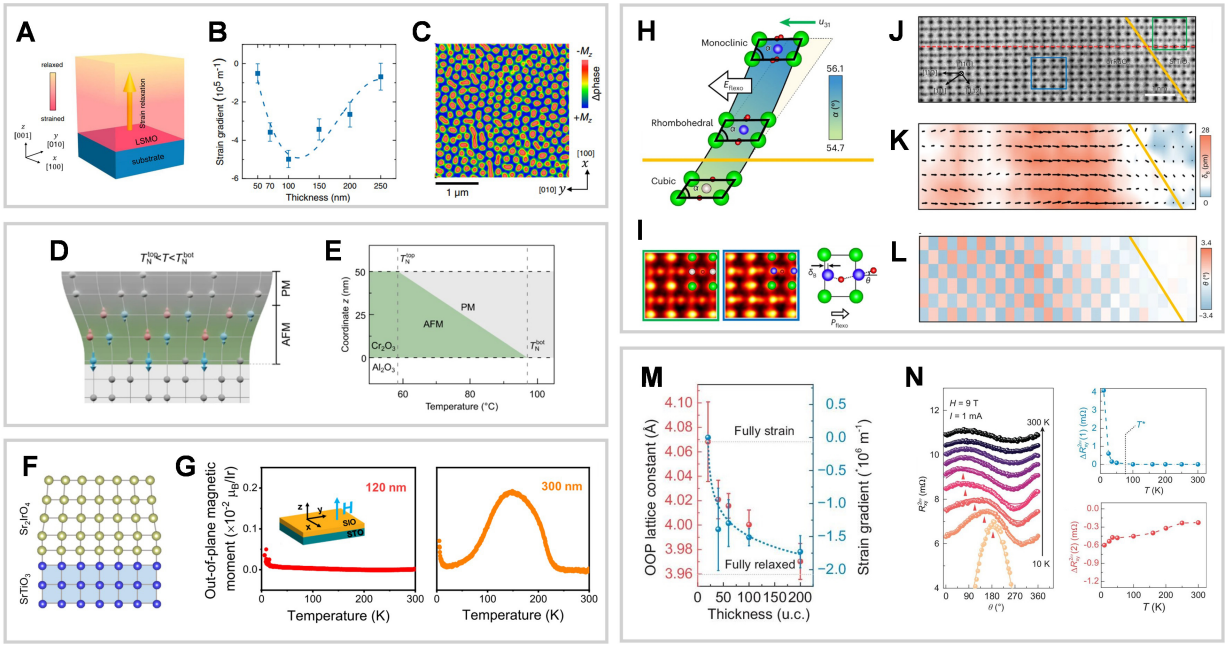

Figure 10. Flexoelectric control of magnetism and spin textures in correlated oxides and ferromagnetic metals. (A-C) Strain-driven Dzyaloshinskii-Moriya interaction in LSMO thin films. (A) Schematic of an epitaxial heterostructure showing tensile strain relaxation across the thickness. (B) Experimentally estimated strain gradient as a function of thickness. (C) Magnetic imaging of a skyrmion lattice at 300 K. (A-C) Reproduced with permission[34]. Copyright 2021, American Physical Society; (D and E) Flexomagnetism in Cr_2O_3 thin films. (D) Illustration of the strain gradient-induced modulation of the Néel temperature across the film thickness. (E) Phase diagram of the antiferromagnetic (AFM)-paramagnetic (PM) transition as a function of temperature and coordinate z. (D and E) Reproduced with permission[75]. Copyright 2022, Springer Nature; (F and G) Flexomagnetoelectric effect in Sr_2IrO_4 thin films. (F) Crystal schematic highlighting broken inversion symmetry and orbital hybridization along the out-of-plane axis. (G) Out-of-plane magnetization as a function of temperature. (F and G) Reproduced with permission[35]. Copyright 2024, American Physical Society; (H-L) Flexoelectric polarization in the ferromagnetic metal $SrRuO_3$. (H) Schematic illustrating shear strain formation and its gradient in a $SrRuO_3/SrTiO_3$ (111) heterostructure. (I) Atomic-scale images of $SrTiO_3$ and $SrRuO_3$ regions corresponding to the boxed areas in (J), showing B-site cation displacement (δ_B) and the projected octahedral tilting angle (θ). (J) Cross-sectional ABF-STEM image of the $SrRuO_3$ layer. (K) Spatial map of cation displacement (δ_B) in (J). (L) Spatial map of octahedral tilt (θ) in (J). (H-L) Reproduced with permission[17]. Copyright 2024, Springer Nature; (M and N) Strain gradient-induced momentum-space spin textures in $SrIrO_3$ thin films. (M) Thickness-dependent strain relaxation and lattice constant variation. (N) Nonlinear magnetoresistance (NLMR) measured as a function of angle and temperature. (M-N) Reproduced with permission[77]. Copyright 2024, Oxford University Press. LSMO: $La_{0.67}Sr_{0.33}MnO_3$; AFM: atomic force microscopy; STEM: scanning transmission electron microscopy; PM: paramagnetic; ABF: annular bright field.

fields, mediated by strong spin-orbit interaction [Figure 10G]. These results revealed a microscopic mechanism for coupled orbital-spin ordering and suggested that flexoelectric symmetry design can be generalized to other centrosymmetric materials with strong electron correlations.

While polarity in metals is traditionally considered ill-defined, Peng *et al.* showed that flexoelectric fields can induce and control bulk polarity in the metallic ferromagnet $SrRuO_3$[17]. Using heteroepitaxial growth, the authors generated shear and longitudinal strain gradients that displaced Ru ions from centrosymmetric positions, generating measurable bulk polarization [Figure 10H and I]. This flexo-polarization was correlated with modifications in electronic bands and enhanced magnetic anisotropy, while maintaining metallic conductivity. High-resolution STEM imaging and first-principles analysis confirmed the persistence of polar displacements across structural domains [Figure 10J-L]. This challenges the conventional incompatibility between polarity and metallicity, demonstrating that flexoelectricity provides a universal pathway to control ferromagnetism in metals without suppressing electronic conduction.

Gu *et al.* also explored how strain gradients impact momentum-space spin textures in nominally centrosymmetric $SrIrO_3$ thin films[77]. Nonlinear magnetoresistance (NLMR) measurements revealed distinct spin splitting in both fully strained and strain-relaxed films. In the film, continuous lattice relaxation

generated gradients that broke inversion symmetry across multiple layers, producing large spin-split bands and anisotropic spin textures in k-space [Figure 10M]. Experimentally, two branches of NLMR signals were observed, corresponding to competing contributions from interface-induced and strain gradient-induced spin splitting [Figure 10N]. Band structure calculations supported this interpretation, demonstrating that flexoelectric strain gradients are efficient drivers of nontrivial spin textures in materials with strong spin-orbit coupling.

Together, these studies firmly establish strain gradients as a powerful mechanism for tailoring magnetism and spin textures over a diverse range of platforms. Their findings can be used to develop a variety of novel device designs, including strain-tunable skyrmionics, reconfigurable antiferromagnetic racetracks, flexomagnetoelectric memory, and spin-orbitronic transistors[79-82]. Flexoelectricity is thus both a means to modulate charge and polarization and a unifying principle for the mechanical control of spin phenomena in correlated materials.

ELECTRIC-FIELD GRADIENT ENGINEERING

Converse flexoelectric effect

While strain gradients can be used to generate polarization and emergent electric fields via the flexoelectric effect, this coupling is fundamentally reciprocal, with a spatial gradient in the electric field having the potential to induce mechanical responses. This converse flexoelectric effect is based on the electric field causing the material to bend, with inhomogeneous polarization generating additional mechanical stress. In Equation (2), the first right-hand-side term is Hook's law with the elastic constant at fixed polarization c, while the second right-hand-side term is the converse flexoelectric response:

$$\sigma = cu + \frac{\mu}{\chi}\frac{\partial P}{\partial x} \tag{2}$$

where μ is the bulk flexoelectric coefficient and χ is the clamped dielectric susceptibility[1,26]. Converse flexoelectricity is allowed by symmetry in all materials, including non-piezoelectric materials, and thus holds promise for use in various fields such as nanoscale actuators, sensors, and flexible electronics[27,52,83].

Methods of electric-field gradient generation

Piezoresponse force microscopy (PFM) is a standard method for generating the converse flexoelectric effect. During the PFM process, where a voltage is delivered to the surface of the material via an electrically conducting tip, the electric field is not evenly distributed, with the field decaying as the tip moves away [Figure 11A].

Work by Abdollahi *et al.* on the effect of flexoelectricity on piezoelectric responses (i.e., the generation of electricity under mechanical stress) during PFM operation has shown that this response is influenced by the size effect[1,26]. This is because flexoelectricity is caused by a strain gradient, meaning a smaller contact surface enhances the gradient, thus inducing a larger deformation. The contact surface area increases as a function of the loading force of the tip, meaning that gradient-induced piezoelectricity is inversely proportional to contact force. This distinguishes the converse flexoelectric response from the regular piezoelectric response because the latter has no dependence on the contact area [Figure 11B][84]. Measurements of the piezoelectric coefficient as a function of the tip loading force in a non-piezoelectric dielectric $SrTiO_3$ show that the relationship is inversely proportional, confirming that converse flexoelectricity is responsible for the large piezoelectric coefficients [Figure 11C].

Other methods used to generate an electric-field gradient for the converse flexoelectric effect include the illumination of a transmission electron microscope (TEM) electron beam or an applied alternating voltage for thin film samples[27,83]. Koirala *et al.* used the illumination of a TEM electron flux to demonstrate

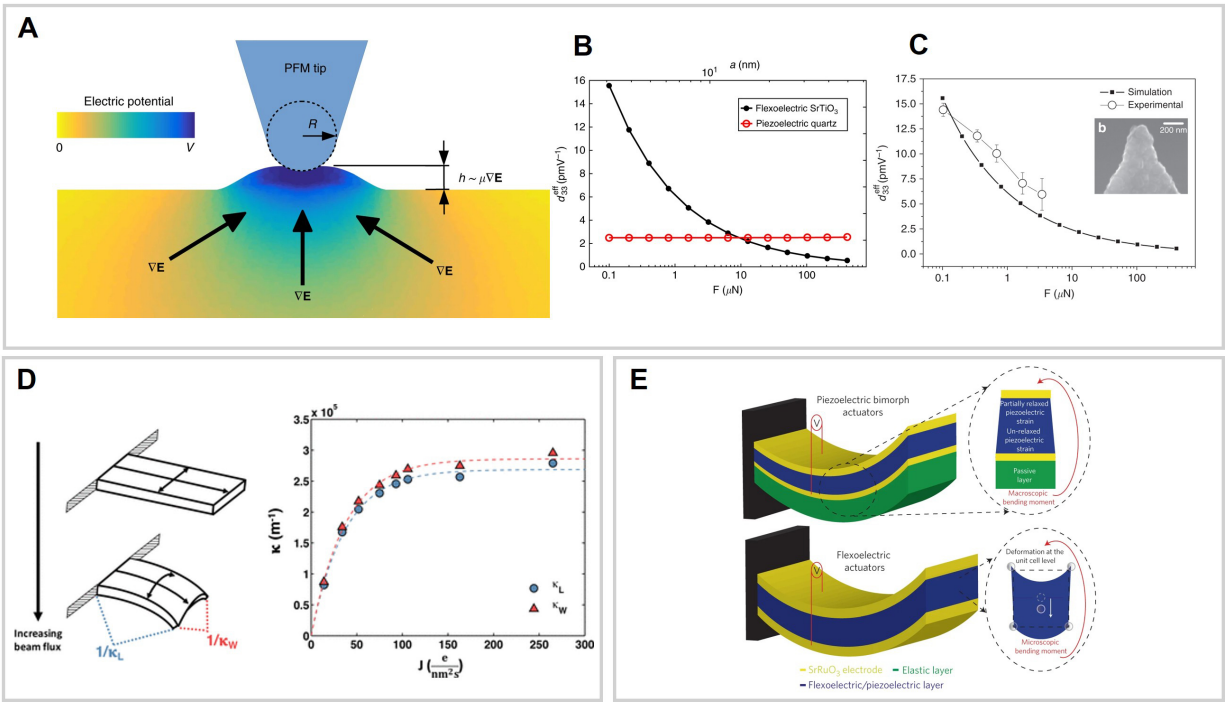

Figure 11. (A) Schematic of piezoresponse force microscopy measurement. (B) Hypothetical response of an archetypal piezoelectric assuming an absence of flexoelectricity. (C) Effective piezoelectric coefficient as a function of applied force for $SrTiO_3$. (A-C) Reproduced with permission[26]. Copyright 2019, Springer Nature; (D) Curvature of a sample bending in response to increasing beam flux. Reproduced with permission[83]. Copyright 2018, American Chemical Society; (E) Schematic of flexoelectric actuation and piezoelectric bimorph actuation in nanoscale actuators. Reproduced with permission[27]. Copyright 2016, Springer Nature. PFM: Piezoresponse force microscopy.

flexoelectric bending in $DyScO_3$ films[83]. Their results showed that the curvature of $DyScO_3$ samples becomes saturated as a function of the electron flux [Figure 11D]. In insulators, charging is net positive for high incident electron energies, resulting in the loss of secondary electrons. The charging scales with the electron flux and is partially compensated by neutralizing processes such as the capture of electrons from other areas. Thus, the top surface of the sample is positively charged with respect to the bottom, resulting in an asymmetric charge distribution and consequently the converse flexoelectric effect.

Applications of the converse flexoelectric effect

The mechanical bending induced by the converse flexoelectric effect is a promising mechanism for actuators. Maier *et al.* constructed a TiO_2-based flexoelectric cantilever and measured the flexoelectric coefficient to be ~1.78 nC m^{-1}[52]. The viability of flexoelectric actuators has also been highlighted by Bhaskar *et al.*, who fabricated a silicon-compatible thin-film cantilever actuator with a single flexoelectrically active layer of $SrTiO_3$ with a figure of merit of 3.33 MV^{-1} [Figure 11E][27].

Converse flexoelectricity also helps to understand ferroelectric domain-wall-related phenomena and other boundaries in ferroelectric materials. Wang *et al.* studied the converse flexoelectric effect around the domain walls in tetragonal ferroelectric $PbTiO_3$ using aberration-corrected TEM, first-principles calculations, and the Landau-Ginzburg-Devonshire (LGD) theory[85]. Their study revealed the important role of converse flexoelectricity in the asymmetric structure around 90° domain walls.

The converse flexoelectric effect illustrates how externally applied electric-field gradients can generate mechanical strain and structural asymmetry in oxide systems. Extending this concept from external-field control to intrinsic material asymmetry, the following section introduces chemical gradient engineering,

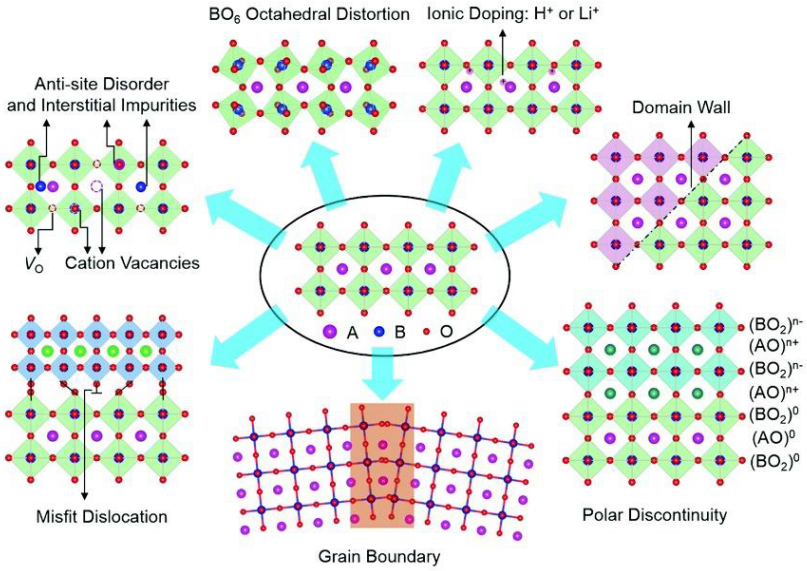

Figure 12. Different types of defects in transition-metal oxides: oxygen vacancies (V_o), missing cation atoms from lattice sites (Vc), misfit dislocation, grain boundaries, polar discontinuities, domain walls, ionic doping, and octahedral distortion. Reproduced with permission[86]. Copyright 2020, The Royal Society of Chemistry.

where spatial variations in defect concentration and composition serve as internal drivers for polarization, strain, and functionality in complex oxides.

CHEMICAL GRADIENT ENGINEERING

Defect gradient engineering

Despite the various physical phenomena induced by strain gradients, conventional approaches such as substrate-induced lattice mismatches, epitaxial thickness variation, or mechanical bending, offer only limited tunability and often suffer from strain relaxation or poor spatial reproducibility. In contrast, chemical gradient engineering provides a more versatile route for the indirect induction of strain gradients by exploiting composition-dependent lattice parameters or defect chemistry, thus controlling strain gradients, defect- and ion-mediated functionalities, built-in electric fields, and enhanced coupling between multiple degrees of freedom.

Complex transition-metal oxides can accommodate a wide range of defects, such as oxygen vacancies (V_o), cation vacancies, local structural distortion, grain boundaries, misfit locations, and impurities [Figure 12][22,23,86-89]. Recent advances in thin-film characterization and synthesis allow precise engineering of these defects to create novel functionalities in oxides. Oxygen vacancies are the most frequent point defects, affecting the structural and transportation properties of oxide thin films[22,23,87,88]. In particular, oxygen vacancies can promote ionic conductivity and significantly distort the equilibrium arrangement of atoms[90]. The presence of oxygen vacancies can also result in an increase in volume, meaning that oxygen vacancy engineering has great potential for use in lattice and strain modulation.

Conventional methods of controlling oxygen vacancies focus on the use of strain engineering. For example, in multiferroic $CaMnO_3$, tensile strain favors the formation of oxygen vacancies. Experiments have shown that the formation energy of oxygen vacancies can be decreased by 0.25 eV with the application of 3.78% tensile strain[24]. First-principles calculations by Aschauer *et al.* showed that the formation energy of oxygen vacancy defects has a strong dependence on strain, which is consistent with the fact that oxygen vacancies increase the molar volume of oxides [Figure 13A][24,91,92]. Furthermore, experiments on $SrTiO_3$ films using an

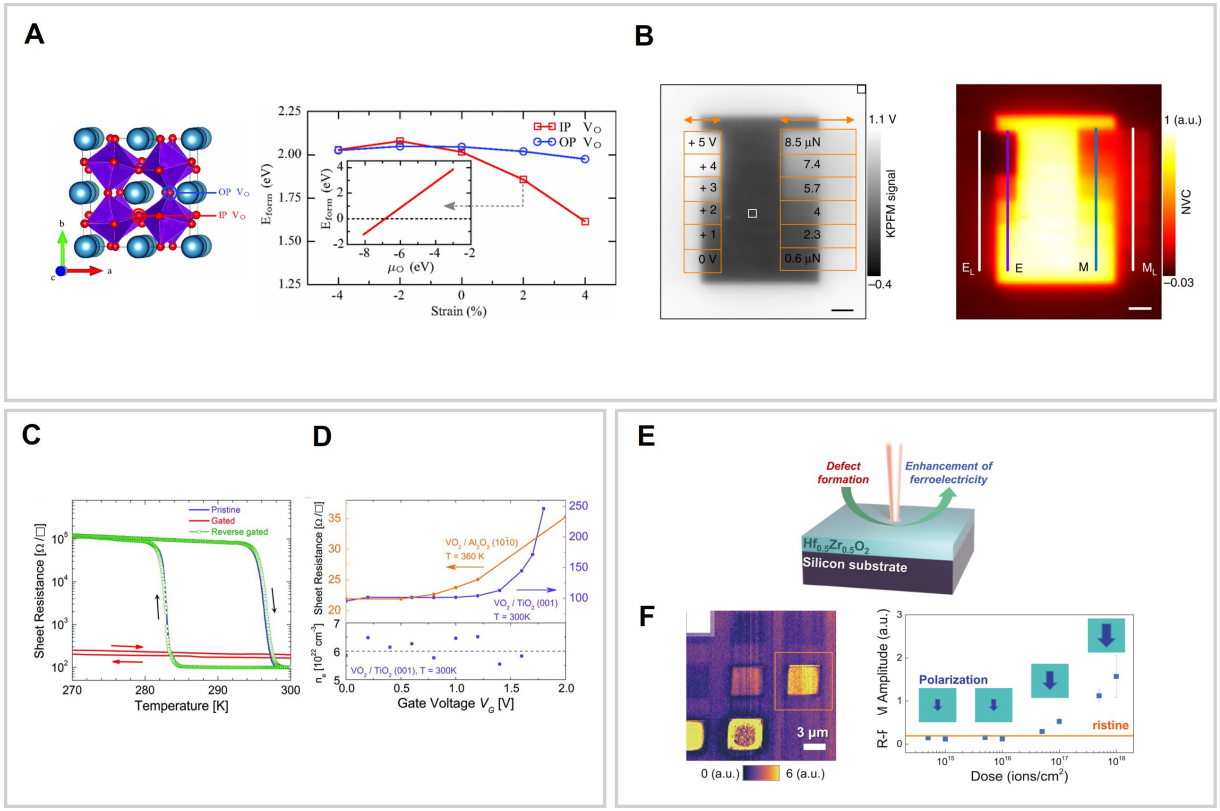

Figure 13. (A) Strain-mediated control of oxygen vacancies. First-principles calculation of the formation energy for oxygen vacancies (V_o) according to the strain in $CaMnO_3$. Reproduced with permission[24]. Copyright 2013, American Physical Society; (B) Strain-mediated control of oxygen vacancies. KPFM image after electrical and mechanical scans between the V_o-enriched and pristine regions. Reproduced with permission[93]. Copyright 2017, Springer Nature; (C) R_s versus T for the same VO_2 device in its pristine state and in gated (1.8 V) and reverse-gated (-0.8 V) states. (D) Sheet resistance for electrolyte-gated devices. (C and D) Reproduced with permission[94]. Copyright 2013, American Association for the Advancement of Science; (E) Ion bombardment-induced creation of V_o. (F) R-PFM image of a HZO thin film after ion bombardment and R-PFM amplitudes. (E and F) Reproduced with permission[95]. Copyright 2022, American Association for the Advancement of Science. KPFM: Kelvin probe force microscope; MIT: metal insulator transition; R-PFM: resonance piezoresponse force microscopy; HZO: hafnium zirconium oxide; NVC: normalised vacancy concentration.

SPM tip demonstrated controlled manipulation of the oxygen vacancy distribution using a mechanical force[93]. The SPM tip created a stress-gradient-induced flexoelectric field, which induced movement in the oxygen vacancies due to the depolarization field [Figure 13B].

The electric-field-induced creation and movement of oxygen vacancy defects is also an active topic of research. Jeong *et al.* showed that electrolyte gating in VO_2 leads to the electric-field-induced creation of oxygen vacancies due to the migration of oxygen from the oxide film into the ionic liquid [Figure 13C and D][94]. Another method for oxygen vacancy creation is ion bombardment, which has been demonstrated in HfO_2 films, with ion bombardment also inducing changes in the ferroelectricity due to local helium implantation [Figure 13E and F][95].

Methods for defect gradient generation

Doping-induced oxygen vacancy gradient engineering

Huang *et al.* demonstrated the use of the Schottky barrier formed at a metal/ferroelectric interface to tailor the self-polarization states of the ferroelectric heterostructure $SrRuO_3$/(Bi,Sm)FeO_3 [Figure 14A][96]. Control of Sm doping in (Bi,Sm)FeO_3 modulates the concentration and spatial distribution of oxygen vacancies[97]. First-principles density functional theory calculations showed that the formation energy of the oxygen

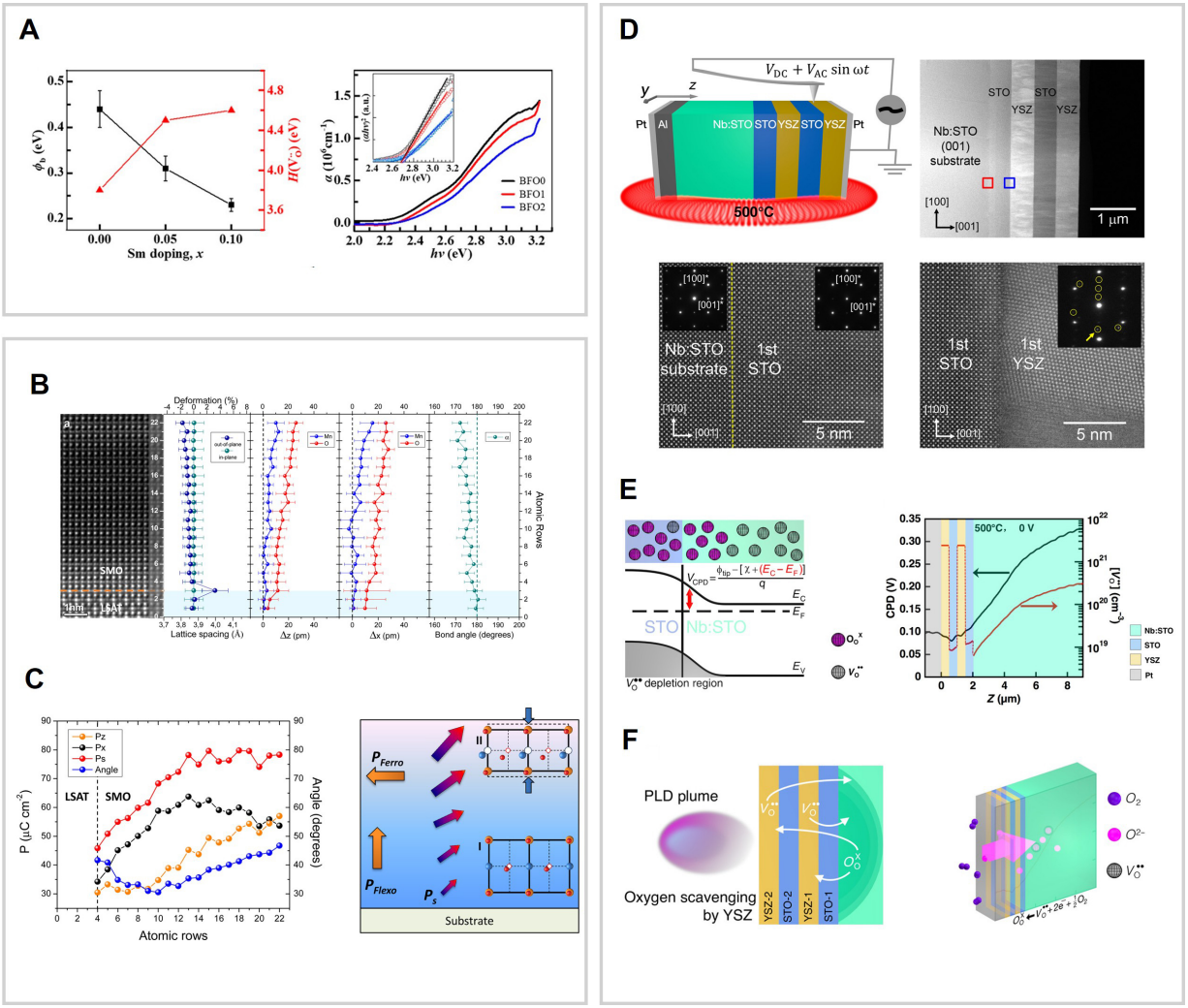

Figure 14. (A) Schottky barriers (left axis) and oxygen-vacancy energy (right axis) plotted as a function of Sm doping content *x*, and absorption coefficients for (Bi,Sm)FeO_3 thin films. Reproduced with permission[96]. Copyright 2023, American Chemical Society; (B) Quantitative analysis of Mn and O displacement and bond angles within an SMO film. (C) Polarization and polar rotation of the SMO structure. Flexoelectricity induced gradual rotation of the in-plane polarization (P_s). (B and C) Reproduced with permission[28]. Copyright 2016, American Chemical Society; (D) Schematic of the *in-situ* potential scanning geometry measurement system and the structure of the multilayer oxide films. (E) Schematic and surface potential profile of the band across the Nb:$SrTiO_3$/$SrTiO_3$ interface. (F) Schematic of PLD-induced substrate reduction and reoxidation. (D-F) Reproduced with permission[100]. Copyright 2019, American Association for the Advancement of Science. SMO: $SrMnO_3$; PLD: pulsed laser deposition; YSZ: yttria-stabilized zirconia; STO: $SrTiO_3$.

vacancy increases from ~3.8 eV to ~4.6 eV with Sm doping. This is due to the smaller ionic radius of Sm compared to that of Bi, reducing the length of the lattice and thus binding strongly with oxygen. Sm doping thus reduces the concentration of oxygen vacancies[97,98]. Notably, the $BiFeO_3$ films start to exhibit polydomain states with Sm doping of 0.05 and 0.1, with the domain area reducing from ~6×10^4 to ~1.6×10^3 nm^2. Considering that the downward electric field due to the interfacial barrier does not support the appearance of upward polarization, the presence of polydomain states indicates that, in addition to the interfacial Schottky barrier, other factors are involved in the formation of the as-grown domain state[99]. In addition, charge screening by oxygen vacancies is considered a competing factor that accounts for the evolution of polydomain states, with incomplete charge screening potentially causing a depolarization field that destabilizes the single domain state.

Strain-induced oxygen vacancy gradient engineering

Research using aberration-corrected STEM in single-phase $SrMnO_3$ (SMO) thin films has proposed that the strain-induced polar gradient is associated with the gradient distribution of oxygen vacancy point defects[28]. Guzman *et al*. probed oxygen deficiencies and the distribution of point defects in an SMO film, using electron energy loss spectroscopy (EELS) to trace the depth profile of the Mn oxidation state[28]. The Mn oxidation state increased gradually toward the top of the film, where the change in the epitaxial tensile strain due to strain relaxation created an oxygen vacancy gradient. While Mn atoms shifted gradually from ~0 pm near the interface to 12 pm deeper in the film, O atoms varied from ~10 pm to 25 pm. The larger displacement of O resulted in a decrease in the Mn-O-Mn bond angle [Figure 14B]. The gradient of bond angles led to variation in the superexchange paths, resulting in local changes in the Néel temperature. The displacements in this new atom arrangement resulted in rotated polarization due to vertical flexoelectricity being coupled to horizontal ferroelectric distortion.

The displacement mapping in Figure 14C shows that the polarization component $P_{z(flexo)}$ appeared to be constant along the in-plane direction, while the $P_{x(ferro)}$ component contained two domains with different polarization. This led to a rotation of the in-plane polarization of about ~15°, resulting in a polarization gradient. Overall, this study demonstrated an oxygen vacancy-mediated route to induce polar rotation.

Probing the vacancy behavior in complex oxide heterointerfaces has become more important in recent years. A study on multilayer $SrTiO_3$/yttria-stabilized zirconia (YSZ)/$SrTiO_3$/YSZ grown on a single-crystal Nb:$SrTiO_3$ substrate demonstrated vacancy distribution gradients within the oxide films due to oxygen scavenging during pulsed laser deposition (PLD)[100]. Zhu *et al.* measured the local surface potential variance orthogonal to the interface of the multilayer $SrTiO_3$/YSZ oxide in cross-sectional films using high-temperature scanning surface potential microscopy (SSPM) [Figure 14D]. The results revealed a reduction in the concentration of oxygen vacancies from ~3.1×10^{20} cm^{-3} in the bulk to 6.3×10^{18} cm^{-3} at the Nb:$SrTiO_3$/$SrTiO_3$ interface [Figure 14E and F]. This study thus presents an approach for controlling oxygen vacancy distribution gradients across scavenging/non-scavenging heterointerfaces to fabricate new functional heterostructures[100,101].

Functionalities of defect gradients

One of the functionalities generated by point defect gradients is the ferroelectric resistive switching behavior shown in $SrRuO_3$/(Bi,Sm)FeO_3/Pt ferroelectric diodes with $Bi_{1-x}Sm_xFeO_3$ (x = 0, 0.05, and 0.1, corresponding to BFO0, BFO1, and BFO2, respectively)[96]. The high oxygen vacancy concentration near the top of BFO0 results in *n*-type heavy doping. The upward polarization after -V poling enhances the ohmic contact of BFO0/Pt and the Schottky barrier at the $SrRuO_3$/BFO0 interface due to the opposite bounding charges at the two interfaces [Figure 15A]. This leads to highly asymmetric I-V conducting behavior, and polarization switching effectively promotes the migration and redistribution of oxygen vacancies in these films [Figure 15B]. Overall, the gradient distribution of oxygen vacancies induced by polarization reversal contributes to a considerable on/off ratio enhancement of ~1.1×10^6 in the BFO0 device [Figure 15C], along with an ultralow writing current density of ~132 A cm^{-2}, a fast writing speed of ~30 ns, and long data retention unprecedented in previously reported systems[102].

Cation vacancy point defects are also a useful control parameter, affecting various properties such as ferroelectricity and the carrier density[22,23,87]. Tracking the combined influence of growth parameters during the PLD growth of ferroelectric $Pb(Zr_{0.2}Ti_{0.8})O_3$ (PZT) using *in-situ* optical second harmonic generation (ISHG), Sarott *et al.* reported that the Pb gradient favored downward polarization with an increase in the oxygen partial pressure and substrate temperature [Figure 15D][103]. For example, when increasing the growth temperature, the enhanced volatility and mobility of Pb led to a Pb gradient across the film thickness. The

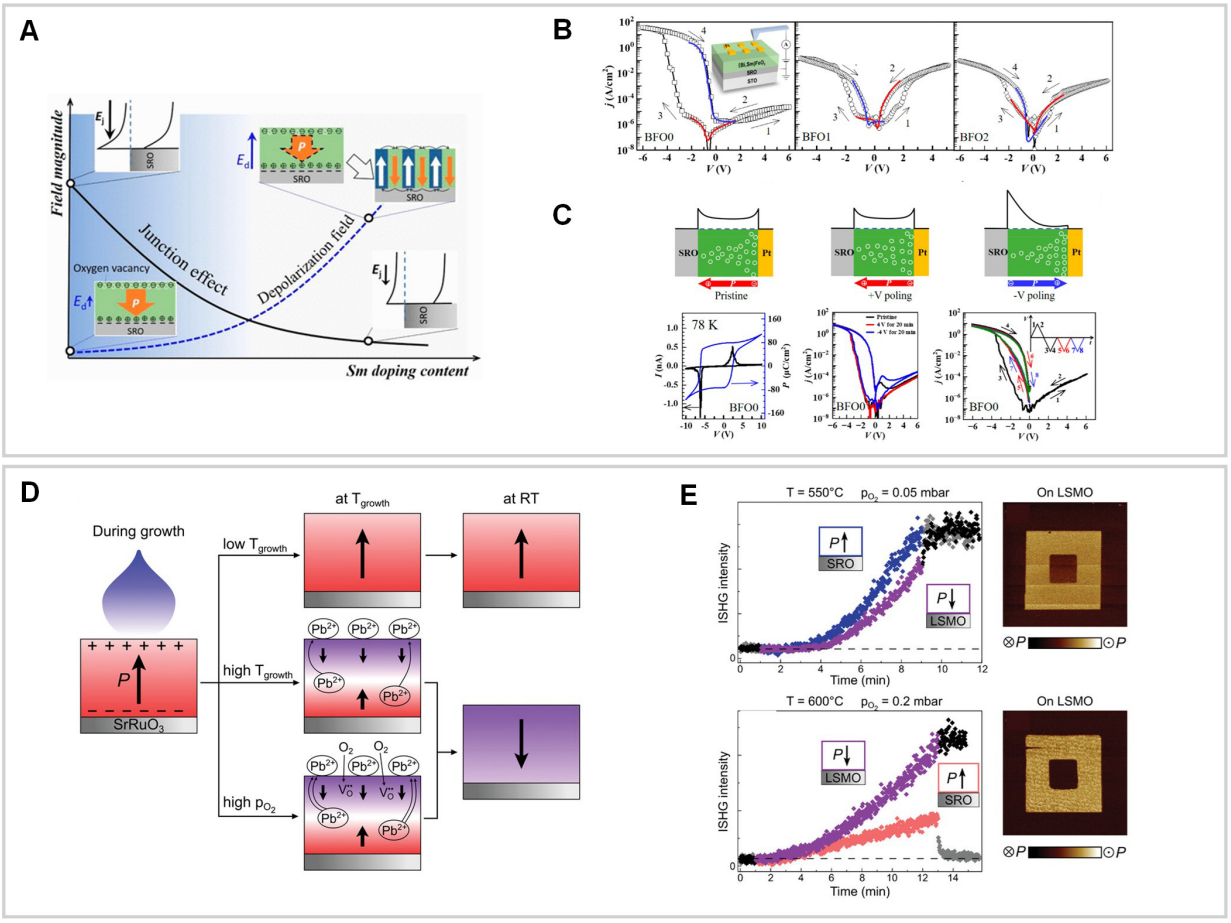

Figure 15. (A) Mechanisms for the self-polarization of (Bi,Sm)FeO_3 films. (B) Resistive-switching behavior of $SrRuO_3$/(Bi,Sm)FeO_3/Pt memristors. I-V characteristics of BFO devices. (C) Schematic energy band diagrams illustrating the variation in the Schottky barriers of back-to-back diodes in polarized down and up states. (A-C) Reproduced with permission[96]. Copyright 2023, American Chemical Society; (D) Interpretation of the evolution of polarization. (E) Influence of the buffer termination on the evolution of polarization. (D and E) Reproduced with permission[103]. Copyright 2023, Wiley-VCH GmbH. LSMO: $La_{0.67}Sr_{0.33}MnO_3$; RT: room temperature; BFO: $BiFeO_3$; SRO: $SrRuO_3$.

positively charged Pb-excess region near the surface then induced downward-oriented polarization [Figure 15E]. This demonstrates that the use of a defect gradient-mediated mechanism controlled by PLD growth parameters can effectively control out-of-plane polarization in ferroelectric PZT thin films.

Doping gradient engineering

Another actively studied method for imposing a chemical gradient on functional oxide thin films is the use of a doping gradient, where the chemical composition of the film is graded across the thickness of the material. On a unit-cell scale, the inversion symmetry of ferroelectric materials is broken. In addition to this, compositionally graded ferroelectric thin films exhibit macroscopically broken inversion symmetry across their thickness[104]. Compared to single-component ferroelectrics, the degeneracy between the two polarized states in these materials is broken by a built-in electric field. These built-in fields can directly affect polarization characteristics and susceptibility in ferroelectrics, leading to potential novel applications such as nonvolatile memories, piezoelectric sensors, and actuators[27,52,83,85,86].

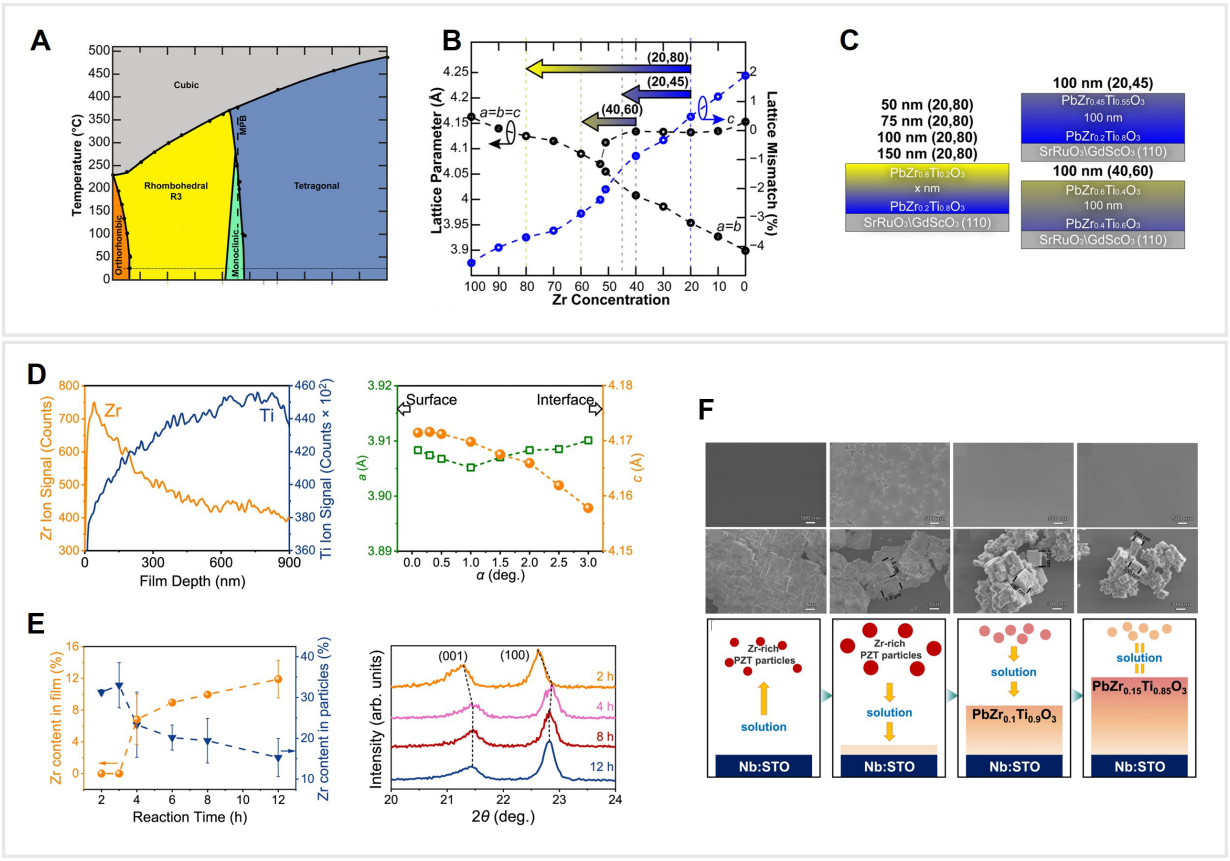

Figure 16. (A) $PbZr_{1-x}Ti_xO_3$ phase diagram. (B) Bulk lattice parameter and calculated misfit strain. (C) Schematics of compositionally graded heterostructures. (A-C) Reproduced with permission[105]. Copyright 2015, American Chemical Society; (D) Characterization of compositionally graded PZT film (TOF-SIMS). (E) Zr/(Zr+Ti) molar ratio of PZT films and particles spontaneously synthesized in the same autoclaves measured using EDS. (F) SEM images of PZT films and particles by the hydrothermal synthesis. Schematic illustrations of the four steps in competitive growth are displayed below. (D-F) Reproduced with permission[107]. Copyright 2025, Springer Nature.

Methods for inducing doping gradients

Compositionally graded heterostructures

Agar *et al.* synthesized the compositionally graded heterostructures $PbZr_{1-x}Ti_xO_3$/30 nm $SrRuO_3$/$GdScO_3$ (110) using pulsed laser deposition from two targets that differed in their composition and a programmable target rotator synced with an excimer laser[105]. Time-of-flight secondary ion mass spectrometry (TOF-SIMS) revealed that the Zr and Ti ion concentration ratio gradually changed over the thickness of the compositionally graded films [Figure 16A and B]. X-ray diffraction reciprocal space mapping (RSM) revealed that up-graded bilayers generally had a tetragonal-like structure, while down-bilayer variants exhibited peaks for both the rhombohedral and tetragonal phases and complete strain relaxation. Imaging of the ferroelectric domain structures of these variants using PFM showed that up-graded films contained structures consisting of out-of-plane and in-plane domains, while the down-graded variants had the domain structure expected for a tensile strained tetragonal phase [Figure 16C]. These results confirmed that compositional gradients can be used to extend the range and strength of strain to a larger extent than would be possible in a single-layer film. In terms of their ferroelectric hysteresis, the up-bilayer and up-graded heterostructures exhibited significantly shifted hysteresis loops and large saturation and remnant polarization. Structural analysis also indicated the preservation of compressive strain in the up-graded films, resulting in strain gradients as large as $4.3 \times 10^5\ m^{-1}$, which led to the generation of a built-in field[105,106].

Zhang *et al.* recently reported a solution epitaxy of compositionally graded $PbZr_xTi_{1-x}O_3$ with a continuous Zr concentration gradient realized by competitive growth[107]. TOF-SIMS revealed a composition gradient where

the Zr content gradually decreased from the surface to the interface [Figure 16D and E]. The growth mechanism for the composition gradient was the competitive relationship between homogeneous nucleation growth of PZT particles and the heteroepitaxy of PZT films on the Nb:$SrTiO_3$ substrate [Figure 16F]. The epitaxial growth of PZT films was suppressed during the initial stage, while the Zr content in the particles was higher than the designed molar ratio of ~10%. When the reaction time was extended, the Zr content in the films increased, while that in the particles decreased. The particles underwent rapid homogeneous nucleation to form pure-phase Zr-rich PZT particles. During subsequent growth of the particles, Ostwald ripening led to the re-dissolution of metastable Zr-rich PZT particles, leading to an increase in the Zr content and promoting the heteroepitaxy of PZT. Accordingly, a composition gradient formed before a dissolution balance was achieved.

Functionalities of doping gradients

Pyroelectric and dielectric properties

The compositional gradients in thin-film heterostructures can independently tune pyroelectric and dielectric responses. Research on compositionally graded $PbZr_{1-x}Ti_xO_3$ revealed strain gradients larger than 10^5 m^{-1} that generated high built-in-potentials that effectively reduced the permittivity while maintaining the large pyroelectric responses[106]. As shown by analysis of polarization-electric field hysteresis loops and dielectric permittivity, the hysteresis loops of compositionally up-graded heterostructures shifted due to the presence of a built-in potential arising from the flexoelectric coupling between the strain gradient and polarization in an out-of-plane direction. A significant difference in the dielectric permittivity was also observed for the single-layer and compositionally graded films. The compositionally down-graded heterostructures exhibited large dielectric permittivity due to their complex domain structure, while the up-graded films were characterized by low dielectric permittivity due to the presence of a built-in potential [Figure 17A]. The single-layer PZT and compositionally up-graded heterostructure had a pyroelectric coefficient of ~229 μC m^{-2} K^{-1}, indicating that the presence of the built-in potential did not influence the pyroelectric response. The down-graded heterostructures had a coefficient of ~185 μC m^{-2} K^{-1} due to the in-plane tetragonal domains contributing a lower pyroelectric current than that of the tetragonal *c* domains in the up-graded films [Figure 17B].

In another study, solution epitaxial competitive growth produced single-domain compositionally graded PZT films with an extremely low dielectric permittivity (~50) and excellent frequency and temperature stability[107]. The low dielectric permittivity enabled the authors to obtain a figure of merit that was ~1.5 times higher than that of conventional PZT films [Figure 17C]. The composition gradient also resulted in a strong photovoltaic effect and pyroelectric current in the ultraviolet and near-infrared range.

Polarization gradients

Damodaran *et al.* demonstrated the manipulation of polarization gradients in $Ba_{1-x}Sr_xTiO_3$ films arising from composition and strain gradients, resulting in spatial polarization gradients as large as 35 μC cm^{-2} across a 150 nm film[108]. High-angle annular dark-field (HAADF)-STEM-based polarization mapping of the compositionally graded heterostructures revealed a tendency for the system to create 180° domain structures as a mechanism for screening depolarization effects that arise from the polarization gradient [Figure 17D]. Dielectric measurements of $Ba_{0.6}Sr_{0.4}TiO_3$ heterostructures revealed a strong temperature-dependent response; in contrast, the compositionally graded heterostructures demonstrated consistently high dielectric permittivity values and high temperature stability [Figure 17E].

Domain structure engineering

Compositionally graded ferroelectric films also show novel features such as highly mobile ferroelastic domain walls. Using controlled composition and strain gradients in compositionally graded $PbZr_{1-x}Ti_xO_3$

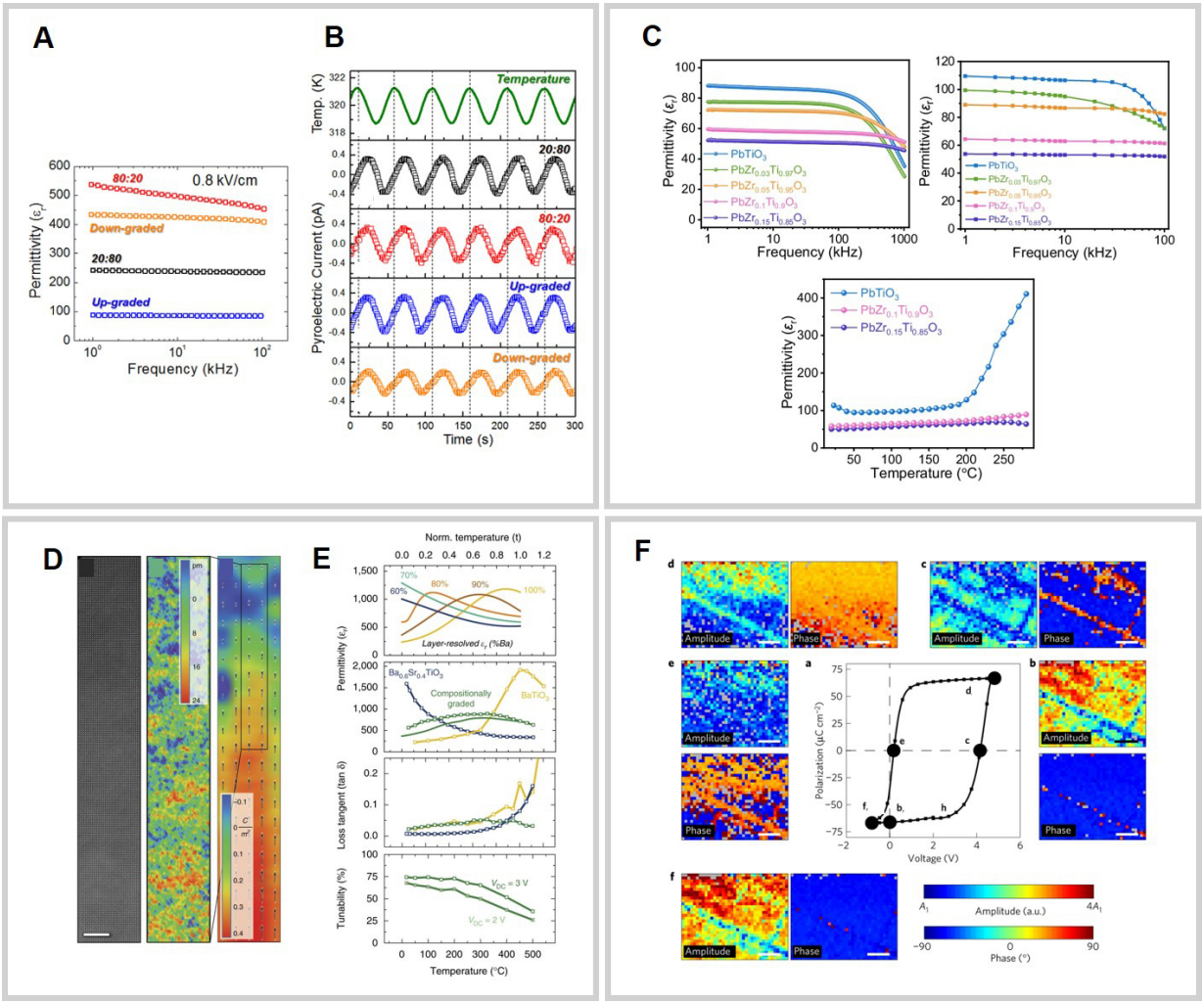

Figure 17. (A) Dielectric permittivity for single-layer and compositionally graded heterostructures. (B) Sinusoidal temperature variation applied to extract the pyroelectric responses of single-layer PZT20:80 and compositionally up-graded and down-graded heterostructures. (A and B) Reproduced with permission[106]. Copyright 2013, American Chemical Society; (C) Dielectric properties of compositionally graded PZT films with an AC excitation voltage of 500 mV. Reproduced with permission[107]. Copyright 2025, Springer Nature; (D) Cross-sectional HAADF-STEM image of the top 72 nm of a compositionally graded heterostructure. (E) Wide-range temperature-stable dielectric permittivity. (D-E) Reproduced with permission[108]. Copyright 2017, Springer Nature; (F) Ferroelectric hysteresis loop of compositionally graded $PbZr_{1-x}Ti_xO_3$ heterostructures and corresponding amplitude and phase images from band-excitation switching spectroscopy at various stages (a-f) of ferroelectric switching. Reproduced with permission[109]. Copyright 2016, Springer Nature. HAADF-STEM: High-angle annular dark-field-scanning transmission electron microscopy; PZT: $PbZr_xTi_{1-x}O_3$.

heterostructures, Agar *et al.* used TEM-based nanobeam diffraction and nanoscale band-excitation switching spectroscopy to demonstrate deterministic control of ferroelastic domains[109]. The compositional and strain gradients preferred the stabilization of needle-like domains that are highly unstable in the out-of-plane direction but remain spatially fixed in plane under successive field cycling. These volatile domain walls led to a locally enhanced piezoresponse as a result of the in-plane polarized domains expanding towards the free surface [Figure 17F].

Synergistic effects of different gradients

Strain, chemical, and field gradients in solids are often interconnected via lattice distortion, charge redistribution, and symmetry breaking. Coupling between these gradients can reinforce or otherwise modify the material response, producing synergistic effects that cannot be replicated with single-gradient engineering. Capturing this interaction is essential for a comprehensive understanding of gradient-driven

functionalities.

Chemical gradients are often coupled with strain gradients. Flexoelectric fields can lead to defect gradients, including cases where an SPM tip creates a stress-gradient-induced flexoelectric field that results in oxygen vacancy movement[93]. Similarly, studies of $SrMnO_3$ have found that a change in the epitaxial tensile strain along the depth of the film creates an oxygen vacancy gradient[28]. Chemical gradients can also lead to large strain gradients due to gradual changes in the lattice parameters, including in compositionally graded films[105,106]. For example, compositionally graded $PbZr_xTi_{1-x}O_3$ has been shown to contain strain gradients as large as 4.3×10^5 m^{-1}, leading to the generation of a built-in field[105].

The synergistic coupling of strain, chemical, and field gradients in oxide thin films can also generate emergent functionalities. While homogeneous doping introduces static disorder without spatial charge redistribution, gradient engineering generates self-reinforcing feedback in which strain gradients induce flexoelectric fields that actively modulate defect migration, establishing a dynamic coupling that is absent when uniform modification is employed. In compositionally graded $PbZr_xTi_{1-x}O_3$, the synergistic interaction between chemical and strain gradients generates built-in polarization fields exceeding those from static doping alone[109]. Unlike heterostructuring, which localizes effects to discrete interfaces, gradient engineering distributes continuous strain gradients across the material volume, simultaneously activating flexoelectricity, oxygen vacancy migration, and polarization switching. Gradient engineering couples multiple order parameters (e.g., lattice distortion, charge density, and polarization) in a spatially-modulated manner, generating collective phenomena in which individual gradient effects are amplified through nonlinear interactions - effects that isolated compositional, mechanical, or electrical perturbations cannot achieve.

FLEXOELECTRICITY IN NON-OXIDE MATERIALS

Although this review primarily focuses on gradient engineering and flexoelectricity in oxide heterostructures, it is important to note that flexoelectric phenomena are not exclusive to oxides. Rather, flexoelectricity is a general electromechanical response to spatial inhomogeneity and has been increasingly observed in non-oxide material systems. For example, recent studies have reported gradient-induced polarization responses in 2D materials[10-13], polymers[46,47], biological materials[14,15], metals[16,17], and ice[48-50].

In 2D materials such as van der Waals crystals[10-12] and transition-metal dichalcogenides[13], flexoelectricity can emerge due to thickness confinement, curvature effects, and interfacial asymmetry. Even modest mechanical deformation or interlayer misalignment can generate large local gradients, producing electromechanical responses absent under uniform strain. Similarly, in polymeric and soft materials, flexoelectric responses arise from bending- or indentation-induced strain gradients combined with a low elastic stiffness, producing measurable signals even with weak mechanical stimuli. This makes polymer platforms attractive for use in soft electromechanical transducers[46], energy-harvesting architectures[47], and flexible wearable sensors[110].

Flexoelectric effects have also been reported in biological materials, where hierarchical structures naturally give rise to intrinsic mechanical gradients, as found in cells[111,112], biomembranes[14], sensory systems such as hearing organs[113], and load-bearing tissues including bone[15,114-116]. These observations suggest a potential role of flexoelectricity in biological sensing and signal transduction. More recently, demonstrations of flexoelectric polarization in metals[16,17] and hydrogen-bonded solids, including ice[48-50], have challenged the conventional view that electromechanical coupling requires insulating or ferroelectric materials. In these systems, local structural or electrostatic gradients can induce polarization even in the presence of a high carrier density or strong hydrogen bonding.

Despite these advances, oxide heterostructures remain one of the most useful platforms for studying and exploiting flexoelectricity due to their structural versatility, chemical tunability, and compatibility with epitaxial growth. In addition, the precise control of strain, field, and chemical gradients and their coupling to other functional degrees of freedom offer a well-defined framework for the development of specific design principles. In particular, the gradient engineering concepts that have been developed using oxide heterostructures, including controlled strain relaxation, interfacial asymmetry, and compositional gradients, offer valuable guidelines for extending flexoelectric functionality to non-oxide materials. Key requirements include the ability to sustain stable spatial gradients and the presence of sufficient electromechanical and/or dielectric responsiveness. In this context, flexoelectricity has the potential to serve as a unifying framework for the generation of gradient-driven functionalities in various oxide and non-oxide material platforms.

CONCLUSIONS

This review systematically analyzed strain[20,25,34,62], field[26,27,83], and chemical gradient engineering[108,109] in oxide materials. As summarized in Table 1, active research in these areas has revealed various promising functionalities. In many cases, these gradients are present at the same time, producing a wide range of novel emergent phenomena. The universality of gradient engineering across a wide range of oxide materials, together with its enhancement at the nanoscale and independence from symmetry constraints, has established it as a versatile design principle for future oxide-based functional materials, with applications that can include energy harvesting, sensing, neuromorphic computing, and sustainable catalysis. In addition, industrial applications of oxide thin-film gradient engineering are increasingly taking advantage of flexoelectricity for use in energy harvesters and self-powered sensors because flexoelectric energy harvesting exhibits a universal presence and can outperform traditional piezoelectrics, which often fail when applied to nanoscale dimensions.

Nevertheless, several fundamental challenges need to be overcome to fully realize the potential of gradient engineered oxide heterostructures. For example, the entanglement of flexoelectric effects with other electromechanical phenomena or interfacial effects - such as intrinsic piezoelectricity arising from defect-induced symmetry breaking[117,118] and ferroelastic domain-wall contributions[119-121] - complicates quantitative analysis and mechanism validation. Current fabrication approaches also struggle to achieve reproducible control of the magnitude and spatial distribution of strain gradients, with gradient profiles varying considerably between samples due to interfacial roughness, relaxation dynamics, and processing-induced defects[122-124]. Furthermore, engineering challenges such as the dynamic stability of gradients under operational conditions need to be addressed to support the development of functional devices. Strain or electrostatic gradients introduced during fabrication may relax or be reconstructed under thermal cycling or the long-term application of an electrical bias, leading to unreliable functionalities[125-127]. Quantifying the lifetime and robustness of these gradients, as well as identifying strategies for stabilized gradient control, is essential. Addressing these challenges is required to both advance the fundamental physical understanding of gradient-induced effects and enable practical device integration.

Recent advancements in *in-situ* and operando characterization techniques such as biasing or bending TEM[128], synchrotron nanodiffraction[129], and spectroscopic probes[130] support the real-time visualization of lattice deformation, defect migration, and polarization evolution under external stimuli. These approaches can be used to quantitatively understand gradient-driven coupling in complex oxides. In parallel, the rapid progress of machine-learning approaches in atomic-resolution imaging and data analysis is opening new possibilities for the optimization of strain gradient designs[131-134]. By extracting structural and electronic information directly from high-resolution datasets, machine learning can accelerate the discovery and control of gradient profiles, offering a pathway toward data-driven material design.

Table 1. Summary of reported strategies to induce the flexoelectric effect by gradient type

Gradient type	Material	Structure	Strain gradient [m^{-1}]	Application	Reference
Strain gradient	$BiFeO_3$	Thin film	3.3×10^7	Flexo-photovoltaic	[20]
	$BiFeO_3$	Film (100 nm)	7.55×10^4	Flexo-photovoltaic	[29]
	$SrTiO_3$	Single crystal	$> 1.0 \times 10^6$	Flexo-photovoltaic	[30]
	TiO_2	Single crystal	$> 1.0 \times 10^6$	Flexo-photovoltaic	[30]
	Ag_2MoO_4	Particle		Flexo-photocatalysis (organic pollutant degradation)	[60]
	$SrTiO_3$	Nanoparticle	2.7×10^6	Flexocatalysis (dye degradation)	[61]
	MnO_2	Nanosheet-assembled nanoflowers	~10^7	Flexocatalysis (organic pollutant degradation)	[62]
	$LaFeO_3$	Thin film	~3.0×10^6	OER	[31]
	$BaTiO_3$	Thin film	~10^8	Polarization switching	[25]
	$CaTiO_3$	Thin film	~10^8	Polarization switching	[67]
	WO_3	Film (~600 nm)	~10^6	Domain tailoring	[32]
	$SrTiO_3$	Thin film	~10^7	Resistivity modulation	[33]
	Nb:$SrTiO_3$	Single crystal		Flexoelectronics	[9]
	TiO_2	Single crystal		Flexoelectronics	[9]
	LSMO	Film (50-200 nm)	~5.0×10^5	Magnetic skyrmion	[34]
	Cr_2O_3	Film (30-250 nm)		Flexomagnetism	[75]
	Sr_2IrO_4	Thin film	1.05×10^6	Flexomagnetoelectric effect	[35]
	$SrRuO_3$	Thin film	3.5×10^6	Ferromagnetic polar metal	[17]
	$SrIrO_3$	Film (~80 nm)	1.75×10^6	Nonlinear magnetoresistance	[77]
Electric-field gradient	TiO_2	Thin film		Flexoelectric cantilever	[52]
	$SrTiO_3$	Thin film		Actuator	[27]
	$PbTiO_3$	Thin film		Domain tailoring	[85]
Chemical gradient	$(Bi,Sm)FeO_3$	Thin film		Ferroelectric resistive switching	[96]
	$Pb(Zr_{0.2}Ti_{0.8})O_3$	Thin film		Polarization control	[103]
	Compositionally graded $PbZr_{1-x}Ti_xO_3$	Thin film	$> 1.0 \times 10^5$	Large dielectric permittivity, pyroelectric coefficient, photovoltaic effect, domain tailoring	[106,109]
	Compositionally graded $PbZr_{1-x}Ti_xO_3$	Film (~900 nm)		High dielectric stability	[107]
	Compositionally graded $Ba_{1-x}Sr_xTiO_3$	Film (150 nm)		Large polarization gradients	[108]

OER: Oxygen evolution reaction.

In the future, gradient engineering is also expected to extend beyond traditional oxide systems to include unconventional materials such as 2D materials[135-137], high-entropy oxides[138-140], hybrid perovskites[8,141], molecular crystals[142], and hydrogen-bonded solids[48-50]. In particular, high-entropy oxides represent a critical platform for gradient engineering, including strain gradients[138] and chemical gradients[139,140]. Recent studies of flexoelectricity in ice[48-50] highlight this emerging research direction, suggesting that gradient-driven

electromechanical phenomena may be far more universal than previously recognized. Nevertheless, for these extensions to be viable, target materials must accommodate spatially non-uniform structural or electrostatic perturbations and exhibit sufficient electromechanical or dielectric responsiveness to translate gradients into functional polarization. Accordingly, the ability to sustain stable strain, electric-field, or chemical gradients is a prerequisite for transferring oxide-based gradient engineering concepts to unconventional materials.

Ultimately, the convergence of strain, electrical, and chemical gradient engineering has established a new paradigm for functional material design, particularly gradient-induced flexoelectricity, and the resulting emergent properties can be intentionally programmed using spatially varying fields. Future research directions should increasingly focus on expanding this paradigm beyond oxide materials, integrating it with low-dimensional and heterogeneous systems, and bridging fundamental discoveries with device-relevant length and time scales.

DECLARATIONS

Authors' contributions

Contributed equally to this work, formal analysis, data curation and writing - original draft: Kim, S.; Kim, Y.
Conceptualization: Lee, D.; Kim, S.; Kim, Y.
Funding acquisition, supervision, validation and writing, review & editing: Lee, D.

Availability of data and materials

Not applicable.

AI and AI-assisted tools statement

During the preparation of this manuscript, the AI tool ChatGPT(OpenAI) (version GPT-5, released 2025 08-07) was used solely for language editing. The tool did not influence the study design, data collection, analysis, interpretation, or the scientific content of the work; The AI tool Nano Banana 2 (version Gemini 3.1 Flash Image, released 2026 02-26) was used for partial creation of the graphical abstract. The tool did not influence the study design, data collection, analysis, interpretation, or the scientific content of the work. All authors take full responsibility for the accuracy, integrity, and final content of the manuscript.

Financial support and sponsorship

This work was supported by a National Research Foundation of Korea (NRF) grant funded by the Korean government (MSIT) (Nos. RS-2021-NR060139, RS-2021-NR060087, RS-2022-NR068223, and RS-2023-NR076846).

Conflicts of interest

All authors declare that there are no conflicts of interest.

Ethical approval and consent to participate

Not applicable.

Consent for publication

Not applicable.

REFERENCES

1. Zubko, P.; Catalan, G.; Tagantsev, A. K. Flexoelectric effect in solids. *Annu. Rev. Mater. Res.* **2013**, *43*, 387-421. DOI
2. Tagantsev, A. K.; Yurkov, A. S. Flexoelectric effect in finite samples. *J. Appl. Phys.* **2012**, *112*, 044103. DOI
3. Tripathy, A.; Saravanakumar, B.; Mohanty, S.; Nayak, S. K.; Ramadoss, A. Comprehensive review on flexoelectric energy harvesting technology: mechanisms, device configurations, and potential applications. *ACS. Appl. Electron. Mater.* **2021**, *3*, 2898-924. DOI
4. Tressler, J. F.; Alkoy, S.; Newnham, R. E. Piezoelectric sensors and sensor materials. *J. Electroceram.* **1998**, *2*, 257-72. DOI

5. Zubko, P.; Catalan, G.; Buckley, A.; Welche, P. R. L.; Scott, J. F. Strain-gradient-induced polarization in $SrTiO_3$ single crystals. *Phys. Rev. Lett.* **2007**, *99*, 167601. DOI
6. Lee, D.; Yoon, A.; Jang, S. Y.; et al. Giant flexoelectric effect in ferroelectric epitaxial thin films. *Phys. Rev. Lett.* **2011**, *107*, 057602. DOI
7. Narvaez, J.; Vasquez-sancho, F.; Catalan, G. Enhanced flexoelectric-like response in oxide semiconductors. *Nature* **2016**, *538*, 219-21. DOI
8. Shu, L.; Ke, S.; Fei, L.; et al. Photoflexoelectric effect in halide perovskites. *Nat. Mater.* **2020**, *19*, 605-9. DOI
9. Wang, L.; Liu, S.; Feng, X.; et al. Flexoelectronics of centrosymmetric semiconductors. *Nat. Nanotechnol.* **2020**, *15*, 661-7. DOI
10. Ming, W.; Huang, B.; Zheng, S.; et al. Flexoelectric engineering of van der Waals ferroelectric $CuInP_2S_6$. *Sci. Adv.* **2022**, *8*, eabq1232. DOI
11. Guo, H.; Yang, T.; Xuan, X.; Zhang, Z.; Guo, W. Flexoelectricity in hexagonal boron nitride monolayers. *Extreme. Mech. Lett.* **2022**, *52*, 101669. DOI
12. Wang, X.; Zhou, X.; Cui, A.; et al. Flexo-photoelectronic effect in n-type/p-type two-dimensional semiconductors and a deriving light-stimulated artificial synapse. *Mater. Horiz.* **2021**, *8*, 1985-97. DOI
13. Jiang, J.; Chen, Z.; Hu, Y.; et al. Flexo-photovoltaic effect in MoS_2. *Nat. Nanotechnol.* **2021**, *16*, 894-901. DOI
14. Mozaffari, K.; Ahmadpoor, F.; Sharma, P. Flexoelectricity and the entropic force between fluctuating fluid membranes. *Math. Mech. Solids.* **2021**, *26*, 1760-78. DOI
15. Núñez-toldrà, R.; Vasquez-sancho, F.; Barroca, N.; Catalan, G. Investigation of the cellular response to bone fractures: evidence for flexoelectricity. *Sci. Rep.* **2020**, *10*, 254. DOI PubMed PMC
16. Yurkov, A. S.; Yudin, P. V. Flexoelectricity in metals. *J. Appl. Phys.* **2021**, *129*, 195108. DOI
17. Peng, W.; Park, S. Y.; Roh, C. J.; et al. Flexoelectric polarizing and control of a ferromagnetic metal. *Nat. Phys.* **2024**, *20*, 450-5. DOI
18. Hwang, H. Y.; Iwasa, Y.; Kawasaki, M.; Keimer, B.; Nagaosa, N.; Tokura, Y. Emergent phenomena at oxide interfaces. *Nat. Mater.* **2012**, *11*, 103-13. DOI
19. Zubko, P.; Gariglio, S.; Gabay, M.; Ghosez, P.; Triscone, J. Interface physics in complex oxide heterostructures. *Annu. Rev. Condens. Matter. Phys.* **2011**, *2*, 141-65. DOI
20. Chu, K.; Jang, B.; Sung, J. H.; et al. Enhancement of the anisotropic photocurrent in ferroelectric oxides by strain gradients. *Nat. Nanotechnol.* **2015**, *10*, 972-9. DOI
21. Catalan, G.; Lubk, A.; Vlooswijk, A. H. G.; et al. Flexoelectric rotation of polarization in ferroelectric thin films. *Nat. Mater.* **2011**, *10*, 963-7. DOI
22. Schooley, J. F.; Hosler, W. R.; Cohen, M. L. Superconductivity in semiconducting $SrTiO_3$. *Phys. Rev. Lett.* **1964**, *12*, 474-5. DOI
23. Yang, Z.; Wang, L.; Dhas, J. A.; et al. Guided anisotropic oxygen transport in vacancy ordered oxides. *Nat. Commun.* **2023**, *14*, 6068. DOI PubMed PMC
24. Aschauer, U.; Pfenninger, R.; Selbach, S. M.; Grande, T.; Spaldin, N. A. Strain-controlled oxygen vacancy formation and ordering in $CaMnO_3$. *Phys. Rev. B.* **2013**, *88*, 054111. DOI
25. Lu, H.; Bark, C.; Esque De Los Ojos, D.; et al. Mechanical writing of ferroelectric polarization. *Science* **2012**, *336*, 59-61. DOI
26. Abdollahi, A.; Domingo, N.; Arias, I.; Catalan, G. Converse flexoelectricity yields large piezoresponse force microscopy signals in non-piezoelectric materials. *Nat. Commun.* **2019**, *10*, 1266. DOI PubMed PMC
27. Bhaskar, U. K.; Banerjee, N.; Abdollahi, A.; et al. A flexoelectric microelectromechanical system on silicon. *Nat. Nanotechnol.* **2015**, *11*, 263-6. DOI
28. Guzmán, R.; Maurel, L.; Langenberg, E.; et al. Polar-graded multiferroic $SrMnO_3$ thin films. *Nano. Lett.* **2016**, *16*, 2221-7. DOI
29. Guo, R.; You, L.; Lin, W.; et al. Continuously controllable photoconductance in freestanding $BiFeO_3$ by the macroscopic flexoelectric effect. *Nat. Commun.* **2020**, *11*, 2571. DOI
30. Yang, M.; Kim, D. J.; Alexe, M. Flexo-photovoltaic effect. *Science* **2018**, *360*, 904-7. DOI
31. Xu, J.; Zhang, X.; Liu, X.; et al. Enhanced oxygen evolution reaction in flexoelectric thin-film heterostructures. *Appl. Phys. Rev.* **2024**, *11*, 041419. DOI
32. Yun, S.; Song, K.; Chu, K.; et al. Flexopiezoelectricity at ferroelastic domain walls in WO_3 films. *Nat. Commun.* **2020**, *11*, 4898. DOI
33. Park, S. M.; Wang, B.; Paudel, T.; et al. Colossal flexoresistance in dielectrics. *Nat. Commun.* **2020**, *11*, 2586. DOI PubMed PMC
34. Zhang, Y.; Liu, J.; Dong, Y.; et al. Strain-driven dzyaloshinskii-moriya interaction for room-temperature magnetic skyrmions. *Phys. Rev. Lett.* **2021**, *127*, 117204. DOI
35. Liu, X.; Hu, T.; Zhang, Y.; et al. Flexomagnetoelectric effect in Sr_2IrO_4 thin films. *Phys. Rev. Lett.* **2024**, *133*, 156505. DOI
36. Mashkevich, V. S.; Tolpygo, K. B. Electrical, optical and elastic properties of diamond type crystals. *Sov. Phys. JETP.* **1957**, *5*, 435-9. https://jetp.ras.ru/cgi-bin/dn/e_005_03_0435.pdf (accessed 2026-05-13).

37. Kogan, S. M. Piezoelectric effect during inhomogeneous deformation and acoustic scattering of carriers in crystals. *Sov. Phys. Solid. State.* **1964**, *5*, 2069-70.
38. Majdoub, M. S.; Sharma, P.; Cagin, T. Enhanced size-dependent piezoelectricity and elasticity in nanostructures due to the flexoelectric effect. *Phys. Rev. B.* **2008**, *77*, 125424. DOI
39. Majdoub, M. S.; Sharma, P.; Çağin, T. Erratum: Enhanced size-dependent piezoelectricity and elasticity in nanostructures due to the flexoelectric effect. *Phys. Rev. B.* **2009**, *79*, 119904. DOI
40. Eliseev, E. A.; Morozovska, A. N.; Glinchuk, M. D.; Blinc, R. Spontaneous flexoelectric/flexomagnetic effect in nanoferroics. *Phys. Rev. B.* **2009**, *79*, 165433. DOI
41. Cross, L. E. Flexoelectric effects: Charge separation in insulating solids subjected to elastic strain gradients. *J. Mater. Sci.* **2006**, *41*, 53-63. DOI
42. Ma, W.; Cross, L. E. Flexoelectricity of barium titanate. *Appl. Phys. Lett.* **2006**, *88*, 232902. DOI
43. Cai, S.; Lun, Y.; Ji, D.; et al. Enhanced polarization and abnormal flexural deformation in bent freestanding perovskite oxides. *Nat. Commun.* **2022**, *13*, 5116. DOI PubMed PMC
44. Yudin, P. V.; Tagantsev, A. K. Fundamentals of flexoelectricity in solids. *Nanotechnology* **2013**, *24*, 432001. DOI
45. Stengel, M. Flexoelectricity from density-functional perturbation theory. *Phys. Rev. B.* **2013**, *88*, 174106. DOI
46. Yan, D.; Wang, J.; Xiang, J.; Xing, Y.; Shao, L. A flexoelectricity-enabled ultrahigh piezoelectric effect of a polymeric composite foam as a strain-gradient electric generator. *Sci. Adv.* **2023**, *9*, eadc8845. DOI PubMed PMC
47. Li, X.; An, Q.; Li, H.; et al. A porous piezoelectric-dielectric flexible energy conversion film for electricity generation from multiple sources. *Chem. Phys. Lett.* **2021**, *767*, 138357. DOI
48. Wen, X.; Ma, Q.; Mannino, A.; Fernandez-serra, M.; Shen, S.; Catalan, G. Flexoelectricity and surface ferroelectricity of water ice. *Nat. Phys.* **2025**, *21*, 1587-93. DOI
49. Wen, X.; Ma, Q.; Liu, J.; Saeed, U.; Shen, S.; Catalan, G. Streaming flexoelectricity in saline ice. *Nat. Mater.* **2025**, *24*, 1533-7. DOI
50. Lee, D. Salt turns ice into a powerful flexoelectric material. *Nat. Mater.* **2025**, *24*, 1511-2. DOI
51. Zhu, J.; Chen, T.; Shu, L.; et al. Flexoelectric fatigue in (K,Na,Li)(Nb,Sb)O_3 ceramics. *Appl. Phys. Lett.* **2018**, *113*, 182901. DOI
52. Maier, F.; Schneider, M.; Schrattenholzer, J.; et al. Flexoelectricity in polycrystalline TiO_2 thin films. *Acta. Mater.* **2020**, *190*, 124-9. DOI
53. Biancoli, A.; Fancher, C. M.; Jones, J. L.; Damjanovic, D. Breaking of macroscopic centric symmetry in paraelectric phases of ferroelectric materials and implications for flexoelectricity. *Nat. Mater.* **2014**, *14*, 224-9. DOI
54. Jeon, B. C.; Lee, D.; Lee, M. H.; et al. Flexoelectric effect in the reversal of self-polarization and associated changes in the electronic functional properties of $BiFeO_3$ thin films. *Adv. Mater.* **2013**, *25*, 5643-9. DOI
55. Guo, R.; Shen, L.; Wang, H.; et al. Tailoring self-polarization of $BaTiO_3$ thin films by interface engineering and flexoelectric effect. *Adv. Mater. Inter.* **2016**, *3*, 1600737. DOI
56. Lee, D.; Jeon, B. C.; Yoon, A.; et al. Flexoelectric control of defect formation in ferroelectric epitaxial thin films. *Adv. Mater.* **2014**, *26*, 5005-11. DOI
57. Lee, D.; Yang, S. M.; Yoon, J.; Noh, T. W. Flexoelectric rectification of charge transport in strain-graded dielectrics. *Nano. Lett.* **2012**, *12*, 6436-40. DOI
58. Park, S. M.; Wang, B.; Das, S.; et al. Selective control of multiple ferroelectric switching pathways using a trailing flexoelectric field. *Nat. Nanotechnol.* **2018**, *13*, 366-70. DOI
59. Kim, K.; Jeong, S.; Chu, K.; et al. Configurable topological textures in strain graded ferroelectric nanoplates. *Nat. Commun.* **2018**, *9*, 403. DOI PubMed PMC
60. Cheng, T.; Gao, H.; Li, R.; Wang, S.; Yi, Z.; Yang, H. Flexoelectricity-induced enhancement in carrier separation and photocatalytic activity of a photocatalyst. *Appl. Surf. Sci.* **2021**, *566*, 150669. DOI
61. Liu, Z.; Wen, X.; Wang, Y.; et al. Robust flexo-catalysis in centrosymmetric nanoparticles. *Adv. Mater. Technol.* **2022**, *7*, 2101484. DOI
62. Wu, T.; Liu, K.; Liu, S.; et al. Highly efficient flexocatalysis of two-dimensional semiconductors. *Adv. Mater.* **2022**, *35*, 2208121. DOI
63. Gómez, A.; Vila-fungueiriño, J. M.; Moalla, R.; et al. Electric and mechanical switching of ferroelectric and resistive states in semiconducting $BaTiO_{3-\delta}$ films on silicon. *Small* **2017**, *13*, 1701614. DOI
64. Lu, H.; Liu, S.; Ye, Z.; et al. Asymmetry in mechanical polarization switching. *Appl. Phys. Lett.* **2017**, *110*, 222903. DOI
65. Lu, H.; Lee, D.; Klyukin, K.; et al. Tunneling hot spots in ferroelectric $SrTiO_3$. *Nano. Lett.* **2017**, *18*, 491-7. DOI
66. Kim, D. J.; Paudel, T. R.; Lu, H.; et al. Room-temperature ferroelectricity in hexagonal $TbMnO_3$ thin films. *Adv. Mater.* **2014**, *26*, 7660-5. DOI
67. Lee, J. H.; Kim, H. J.; Yoon, J.; et al. Flexoelectricity-driven mechanical switching of polarization in metastable ferroelectrics. *Phys. Rev. Lett.* **2022**, *129*, 117601. DOI

68. Das, S.; Wang, B.; Paudel, T. R.; et al. Enhanced flexoelectricity at reduced dimensions revealed by mechanically tunable quantum tunnelling. *Nat. Commun.* **2019**, *10*, 537. DOI PubMed PMC
69. Lenzner, M.; Krüger, J.; Sartania, S.; et al. Femtosecond optical breakdown in dielectrics. *Phys. Rev. Lett.* **1998**, *80*, 4076-9. DOI
70. Zener, C. A theory of the electrical breakdown of solid dielectrics. *Proc. A.* **1934**, *145*, 523-9. DOI
71. Trung, T. Q.; Lee, N. E. Flexible and stretchable physical sensor integrated platforms for wearable human-activity monitoringand personal healthcare. *Adv. Mater.* **2016**, *28*, 4338-72. DOI
72. Tang, Z.; Gong, Q.; Yi, M. Flexomagnetism: progress, challenges, and opportunities. *Mater. Sci. Eng. R. Rep.* **2025**, *162*, 100878. DOI
73. Gong, Q.; Tang, Z.; Yi, M. Large flexomagnetic response enabled by topological magnetic textures in monolayer CrN. *Phys. Rev. B.* **2025**, *111*, 094441. DOI
74. Liu, L.; Chen, W.; Zheng, Y. Flexoresponses of synthetic antiferromagnetic systems hosting skyrmions. *Phys. Rev. Lett.* **2022**, *128*, 257201. DOI
75. Makushko, P.; Kosub, T.; Pylypovskyi, O. V.; et al. Flexomagnetism and vertically graded Néel temperature of antiferromagnetic Cr_2O_3 thin films. *Nat. Commun.* **2022**, *13*, 6745. DOI
76. Zhang, J.; Shen, S.; Puggioni, D.; et al. A correlated ferromagnetic polar metal by design. *Nat. Mater.* **2024**, *23*, 912-9. DOI
77. Gu, M.; Sheng, H.; Wu, X.; et al. Momentum-space spin texture induced by strain gradient in nominally centrosymmetric $SrIrO_3$ films. *Natl. Sci. Rev.* **2024**, *11*, nwad296. DOI
78. Li, J.; Simensen, H.; Reitz, D.; et al. Observation of magnon polarons in a uniaxial antiferromagnetic insulator. *Phys. Rev. Lett.* **2020**, *125*, 217201. DOI
79. Shen, Z.; Song, C.; Xue, Y.; Wu, Z.; Wang, J.; Zhong, Z. Strain-tunable dzyaloshinskii-moriya interaction and skyrmions in two-dimensional Janus $Cr_2X_3Y_3$ (X, Y = Cl, Br, I, $X \neq Y$) trihalide monolayers. *Phys. Rev. B.* **2022**, *106*, 094403. DOI
80. Gu, K.; Guan, Y.; Hazra, B. K.; et al. Three-dimensional racetrack memory devices designed from freestanding magnetic heterostructures. *Nat. Nanotechnol.* **2022**, *17*, 1065-71. DOI PubMed PMC
81. Jani, H.; Harrison, J.; Hooda, S.; et al. Spatially reconfigurable antiferromagnetic states in topologically rich free-standing nanomembranes. *Nat. Mater.* **2024**, *23*, 619-26. DOI PubMed PMC
82. Trier, F.; Noël, P.; Kim, J.; Attané, J.; Vila, L.; Bibes, M. Oxide spin-orbitronics: spin-charge interconversion and topological spin textures. *Nat. Rev. Mater.* **2021**, *7*, 258-74. DOI
83. Koirala, P.; Mizzi, C. A.; Marks, L. D. Direct observation of large flexoelectric bending at the nanoscale in lanthanide scandates. *Nano. Lett.* **2018**, *18*, 3850-6. DOI
84. Morozovska, A. N.; Eliseev, E. A.; Svechnikov, G. S.; Kalinin, S. V. Nanoscale electromechanics of paraelectric materials with mobile charges: size effects and nonlinearity of electromechanical response of $SrTiO_3$ films. *Phys. Rev. B.* **2011**, *84*, 045402. DOI
85. Wang, Y.; Tang, Y.; Zhu, Y.; Feng, Y.; Ma, X. Converse flexoelectricity around ferroelectric domain walls. *Acta. Mater.* **2020**, *191*, 158-65. DOI
86. Li, W.; Shi, J.; Zhang, K. H. L.; Macmanus-driscoll, J. L. Defects in complex oxide thin films for electronics and energy applications: challenges and opportunities. *Mater. Horiz.* **2020**, *7*, 2832-59. DOI
87. Koonce, C. S.; Cohen, M. L.; Schooley, J. F.; Hosler, W. R.; Pfeiffer, E. R. Superconducting transition temperatures of semiconducting $SrTiO_3$. *Phys. Rev.* **1967**, *163*, 380-90. DOI
88. Rice, W. D.; Ambwani, P.; Bombeck, M.; et al. Persistent optically induced magnetism in oxygen-deficient strontium titanate. *Nat. Mater.* **2014**, *13*, 481-7. DOI
89. Lu, N.; Zhang, P.; Zhang, Q.; et al. Electric-field control of tri-state phase transformation with a selective dual-ion switch. *Nature* **2017**, *546*, 124-8. DOI
90. Cazorla, C. Lattice effects on the formation of oxygen vacancies in perovskite thin films. *Phys. Rev. Appl.* **2017**, *7*, 044025. DOI
91. Agrawal, P.; Guo, J.; Yu, P.; et al. Strain-driven oxygen deficiency in multiferroic $SrMnO_3$ thin films. *Phys. Rev. B.* **2016**, *94*, 104101. DOI
92. Marthinsen, A.; Grande, T.; Selbach, S. M. Microscopic link between electron localization and chemical expansion in $AMnO_3$ and $ATiO_3$ perovskites (A = Ca, Sr, Ba). *J. Phys. Chem. C.* **2020**, *124*, 12922-32. DOI
93. Das, S.; Wang, B.; Cao, Y.; et al. Controlled manipulation of oxygen vacancies using nanoscale flexoelectricity. *Nat. Commun.* **2017**, *8*, 615. DOI
94. Jeong, J.; Aetukuri, N.; Graf, T.; Schladt, T. D.; Samant, M. G.; Parkin, S. S. P. Suppression of metal-insulator transition in VO_2 by electric field-induced oxygen vacancy formation. *Science* **2013**, *339*, 1402-5. DOI
95. Kang, S.; Jang, W.; Morozovska, A. N.; et al. Highly enhanced ferroelectricity in HfO_2-based ferroelectric thin film by light ion bombardment. *Science* **2022**, *376*, 731-8. DOI

96. Huang, B.; Zhao, X.; Li, X.; et al. Schottky barrier control of self-polarization for a colossal ferroelectric resistive switching. *ACS. Nano.* **2023**, *17*, 12347-57. DOI
97. Clark, S. J.; Robertson, J. Energy levels of oxygen vacancies in $BiFeO_3$ by screened exchange. *Appl. Phys. Lett.* **2009**, *94*, 022902. DOI
98. Yang, T.; Wei, J.; Guo, Y.; Lv, Z.; Xu, Z.; Cheng, Z. Manipulation of oxygen vacancy for high photovoltaic output in bismuth ferrite films. *ACS. Appl. Mater. Interfaces.* **2019**, *11*, 23372-81. DOI
99. Mehta, R. R.; Silverman, B. D.; Jacobs, J. T. Depolarization fields in thin ferroelectric films. *J. Appl. Phys.* **1973**, *44*, 3379-85. DOI
100. Zhu, J.; Lee, J.; Lee, H.; et al. Probing vacancy behavior across complex oxide heterointerfaces. *Sci. Adv.* **2019**, *5*, eaau8467. DOI
101. Chen, Y.; Pryds, N.; Kleibeuker, J. E.; et al. Metallic and insulating interfaces of amorphous $SrTiO_3$-based oxide heterostructures. *Nano. Lett.* **2011**, *11*, 3774-8. DOI
102. Zahoor, F.; Azni Zulkifli, T. Z.; Khanday, F. A. Resistive random access memory (RRAM): an overview of materials, switching mechanism, performance, multilevel cell (mlc) storage, modeling, and applications. *Nanoscale. Res. Lett.* **2020**, *15*, 90. DOI
103. Sarott, M. F.; Bucheli, U.; Lochmann, A.; Fiebig, M.; Trassin, M. Controlling the polarization in ferroelectric PZT films via the epitaxial growth conditions. *Adv. Funct. Mater.* **2023**, *33*, 2214849. DOI
104. Karthik, J.; Mangalam, R. V. K.; Agar, J. C.; Martin, L. W. Large built-in electric fields due to flexoelectricity in compositionally graded ferroelectric thin films. *Phys. Rev. B.* **2013**, *87*, 024111. DOI
105. Agar, J. C.; Damodaran, A. R.; Velarde, G. A.; Pandya, S.; Mangalam, R. V. K.; Martin, L. W. Complex evolution of built-in potential in compositionally-graded $PbZr_xTi_xO_3$ thin films. *ACS. Nano.* **2015**, *9*, 7332-42. DOI
106. Mangalam, R. V. K.; Agar, J. C.; Damodaran, A. R.; Karthik, J.; Martin, L. W. Improved pyroelectric figures of merit in compositionally graded $PbZr_xTi_xO_3$ thin films. *ACS. Appl. Mater. Interfaces.* **2013**, *5*, 13235-41. DOI
107. Zhang, R.; Lin, C.; Dong, H.; et al. Compositionally-graded ferroelectric thin films by solution epitaxy produce excellent dielectric stability. *Nat. Commun.* **2025**, *16*, 98. DOI
108. Damodaran, A. R.; Pandya, S.; Qi, Y.; et al. Large polarization gradients and temperature-stable responses in compositionally-graded ferroelectrics. *Nat. Commun.* **2017**, *8*, 14961. DOI
109. Agar, J. C.; Damodaran, A. R.; Okatan, M. B.; et al. Highly mobile ferroelastic domain walls in compositionally graded ferroelectric thin films. *Nat. Mater.* **2016**, *15*, 549-56. DOI
110. Le Scornec, J.; Guiffard, B. Large curvature sensors based on flexoelectric effect in PEDOT:PSS polymer films. *ACS. Mater. Lett.* **2023**, *5*, 2929-41. DOI
111. Venkateshwarlu, A. Akshayveer, .; Singh, S.; Melnik, R. Piezoelectricity and flexoelectricity in biological cells: the role of cell structure and organelles. *Biomech. Model. Mechanobiol.* **2024**, *24*, 47-76. DOI
112. Singh, S.; Krishnaswamy, J. A.; Melnik, R. Biological cells and coupled electro-mechanical effects: the role of organelles, microtubules, and nonlocal contributions. *J. Mech. Behav. Biomed. Mater.* **2020**, *110*, 103859. DOI
113. Galassi, V. V.; Wilke, N. On the coupling between mechanical properties and electrostatics in biological membranes. *Membranes* **2021**, *11*, 478. DOI
114. Ganghoffer, J. F.; Do, X. N.; Ibrahimbegovic, A. Thermodynamic formulations of the growth of solid bodies subjected to electromechanical interactions and application to bone external and internal remodeling. *Continuum. Mech. Thermodyn.* **2021**, *33*, 1567-602. DOI
115. Witt, C.; Kaiser, T.; Menzel, A. Modelling and numerical simulation of remodelling processes in cortical bone: an IGA approach to flexoelectricity-induced osteocyte apoptosis and subsequent bone cell diffusion. *J. Mech. Phys. Solids.* **2023**, *173*, 105194. DOI
116. Witt, C.; Kaiser, T.; Menzel, A. An IGA-FEA model for flexoelectricity-induced healing of microcracks in cortical bone. *Comput. Methods. Appl. Mech. Eng.* **2024**, *425*, 116919. DOI
117. Park, D.; Hadad, M.; Riemer, L. M.; et al. Induced giant piezoelectricity in centrosymmetric oxides. *Science* **2022**, *375*, 653-7. DOI
118. Yang, M.; Zhu, T.; Renz, A. B.; et al. Auxetic piezoelectric effect in heterostructures. *Nat. Mater.* **2023**, *23*, 95-100. DOI
119. Jones, J. L.; Hoffman, M.; Daniels, J. E.; Studer, A. J. Direct measurement of the domain switching contribution to the dynamic piezoelectric response in ferroelectric ceramics. *Appl. Phys. Lett.* **2006**, *89*, 092901. DOI
120. Schultheiß, J.; Rojac, T.; Meier, D. Unveiling alternating current electronic properties at ferroelectric domain walls. *Adv. Elect. Mater.* **2021**, *8*, 2100996. DOI
121. Bell, A. J.; Shepley, P. M.; Li, Y. Domain wall contributions to piezoelectricity in relaxor-lead titanate single crystals. *Acta. Mater.* **2020**, *195*, 292-303. DOI
122. Huff, M. Review paper: residual stresses in deposited thin-film material layers for micro- and nano-systems manufacturing. *Micromachines* **2022**, *13*, 2084. DOI
123. Webb, M.; Ma, T.; Hunter, A. H.; et al. Geometric defects induced by strain relaxation in thin film oxide superlattices. *J. Appl. Phys.* **2022**, *132*, 185307. DOI

124. Wu, M.; Zhang, X.; Li, X.; et al. Engineering of atomic-scale flexoelectricity at grain boundaries. *Nat. Commun.* **2022**, *13*, 216. DOI
125. Wang, L.; Yang, Z.; Wu, J.; et al. Time- and strain-dependent nanoscale structural degradation in phase change epitaxial strontium ferrite films. *npj. Mater. Degrad.* **2020**, *4*, 16. DOI
126. Li, J.; Han, Z.; Liu, J.; Zou, Y.; Xu, X. Compositional gradient engineering and applications in halide perovskites. *Chem. Commun.* **2023**, *59*, 5156-73. DOI
127. Langenberg, E.; Maurel, L.; Antorrena, G.; Algarabel, P. A.; Magén, C.; Pardo, J. A. Relaxation mechanisms and strain-controlled oxygen vacancies in epitaxial $SrMnO_3$ films. *ACS. Omega.* **2021**, *6*, 13144-52. DOI
128. Li, K.; Bu, Y.; Wang, H. Advances on in situ TEM mechanical testing techniques: a retrospective and perspective view. *Front. Mater.* **2023**, *10*, 1207024. DOI
129. Ahn, Y.; Cherukara, M. J.; Cai, Z.; et al. X-ray nanodiffraction imaging reveals distinct nanoscopic dynamics of an ultrafast phase transition. *Proc. Natl. Acad. Sci. U.S.A.* **2022**, *119*, e2118597119. DOI
130. Ji, Q.; Tang, B.; Zhang, X.; et al. Operando identification of the oxide path mechanism with different dual-active sites for acidic water oxidation. *Nat. Commun.* **2024**, *15*, 8089. DOI
131. Kim, J. R.; Jang, J.; Go, K.; et al. Stabilizing hidden room-temperature ferroelectricity via a metastable atomic distortion pattern. *Nat. Commun.* **2020**, *11*, 4944. DOI
132. Han, J.; Go, K.; Jang, J.; Yang, S.; Choi, S. Materials property mapping from atomic scale imaging via machine learning based sub-pixel processing. *npj. Comput. Mater.* **2022**, *8*, 196. DOI
133. Smalley, D.; Lough, S. D.; Holtzman, L. N.; et al. Determining the density and spatial descriptors of atomic scale defects of 2H-WSe_2 with ensemble deep learning. *APL. Machine. Learning.* **2024**, *2*, 036104. DOI
134. Zhu, M.; Lanier, J.; Flores, J.; et al. Structural degeneracy and formation of crystallographic domains in epitaxial $LaFeO_3$ films revealed by machine-learning assisted 4D-STEM. *Sci. Rep.* **2024**, *14*, 4198. DOI
135. Blundo, E.; Cappelluti, E.; Felici, M.; Pettinari, G.; Polimeni, A. Strain-tuning of the electronic, optical, and vibrational properties of two-dimensional crystals. *Appl. Phys. Rev.* **2021**, *8*, 021318. DOI
136. Ren, H.; Xiang, G. Strain engineering of intrinsic ferromagnetism in 2D van der Waals materials. *Nanomaterials* **2023**, *13*, 2378. DOI
137. Wang, E.; Chen, Z.; Shi, R.; et al. Humidity-controlled dynamic engineering of buckling dimensionality in MoS_2 thin films. *ACS. Nano.* **2022**, *16*, 14157-67. DOI
138. Zhang, Y.; Ren, K.; Wang, W. Y.; et al. Smart design $A_2Zr_2O_7$-type high-entropy oxides through lattice-engineering toughening strategy. *npj. Comput. Mater.* **2024**, *10*, 277. DOI
139. Wang, L.; Koirala, K. P.; Wu, S.; et al. Selective oxidation and cr segregation in high-entropy oxide thin films. *Nano. Lett.* **2025**, *25*, 12719-27. DOI
140. Strotkötter, V.; Krysiak, O. A.; Zhang, J.; et al. Discovery of high-entropy oxide electrocatalysts: from thin-film material libraries to particles. *Chem. Mater.* **2022**, *34*, 10291-303. DOI
141. Xiong, Y.; Luo, Z.; Chen, W.; et al. Atomic-scale insights into flexoelectricity and the enhanced photovoltaic effect at the grain boundary in halide perovskites. *Nano. Lett.* **2025**, *25*, 9734-40. DOI
142. Škarabot, M.; Mottram, N. J.; Kaur, S.; et al. Flexoelectric polarization in a nematic liquid crystal enhanced by dopants with different molecular shape polarities. *ACS. Omega.* **2022**, *7*, 9785-95. DOI